INCOHERENT SOURCES FOR RESONANCE RAMAN SPECTROMETRY

By

CHONYU CHEN

A DISSERTATION PRESENTED TO THE GRADUATE SCHOOL
OF THE UNIVERSITY OF FLORIDA IN PARTIAL FULFILLMENT
OF THE REQUIREMENTS FOR THE DEGREE OF
DOCTOR OF PHILOSOPHY

UNIVERSITY OF FLORIDA

1994

Dedicated to my parents, sisters, brothers, and wife
for their love, and support.

ACKNOWLEDGEMENTS

I would like to acknowledge and thank to Dr. Jim Winefordner for his patience and advice throughout my graduate school career. Without his support and guidance this work would not have been possible.

I also would like to express my thanks to Procter & Gamble Company for financial assistance to this project and Dr. M.J. Pelletier for his useful suggestions during the course of this work.

Many members of the group, both past and present, have helped me during my graduate studies. They are too many to mention individually; thanks go to all of them. However, I am especially grateful to Drs. Ben Smith and Giuseppe Petrucci for their continued and patient assistance in every aspect of this research and for solving some problems encountered during the project.

My thanks also go to Dennis Hueber for helping me with the computer program, Bill Spencer, Anil Raghani, and Stefanie Pagano for reviewing my manuscript and my good friend, Chen-Chan Hsueh, for discussion of my research.

Finally, I am deeply indebted to my family and my wife, Chiuchuan, for their love, encouragement, and understanding throughout my studies.

TABLE OF CONTENTS

LIST OF TABLES

LIST OF FIGURES

Abstract of Dissertation Presented to the Graduate School
of the University of Florida in Partial Fulfillment of the
Requirements for the Degree of Doctor of Philosophy

INCOHERENT SOURCES FOR RESONANCE RAMAN SPECTROMETRY

By

Chonyu Chen

April 1994

Chairman: Dr. James D. Winefordner
Major Department: Chemistry

Ultraviolet resonance Raman spectrometry can overcome the limitations of normal Raman spectrometry due to fluorescence background and weak Raman scattering. Pulsed laser systems (excimer or Nd-YAG) or continuous wave (CW) laser systems (frequency-doubled argon-ion laser) are currently used as excitation sources. Such systems are complicated and expensive. Furthermore, the high peak power from pulsed lasers may cause nonlinear and saturation effects.

The purpose of this research was to evaluate simple and inexpensive incoherent sources and to design a sample cell for an ultraviolet resonance Raman spectrometer. Several different incoherent sources such as the Hg Pen-Ray lamp, Zn Pen-Ray lamp,

Cd Pen-Ray lamp, and the Hg electrodeless discharge lamp have been evaluated. Three flowing sample cells were tested and compared. The best instrumental conditions were obtained by optimizing the sample flow rate, photomultiplier tube high voltage, and sample cell image position. A simulated model was calculated by a computer program and the results were compared to the absorption experiments.

Polycyclic aromatic hydrocarbons (PAHs) are highly carcinogenic; they are also Raman scattering compounds. Several resonance Raman spectra of PAHs and their derivatives have been successfully measured by this experimental setup. By correcting the excitation irradiance for absorption, anthracene can be quantitatively determined over several orders of magnitude; a detection limit of about 0.4 ppm was obtained.

CHAPTER 1
AN INTRODUCTION TO RAMAN EFFECT

Background

The Raman effect was first predicted on theoretical ground in 1923 by A. Smekal [1]. The announcement of the first discovery of this phenomenon was made by C.V. Raman on March 1928, at a meeting of the South India Science Association at Bangalore [2]. In the very first experiment, Raman used sunlight and a pair of complementary filters having fairly narrow regions of transmission; later, he used the conventional mercury arc as an excitation source. In a series of papers [3,4,5], C.V. Raman and K.S. Krishnan reported results obtained with liquids, gases, crystals, and amorphous substances like glass and the scattered light was dispersed by a glass prism and detected by eyes or a photographic plate. The importance of these works was recognized by awarding Raman a Nobel Prize in physics in 1930.

After the discovery of the Raman effect, during 1928-1940, the number of papers published on various aspects of the phenomenon was more than 1800, with more than 2500 different substances investigated [6]. In these early stages, the interest changed from an explanation of the Raman effect to structural and constitutional information. During 1940-1960 (before the laser was invented), considerable progress was made in our knowledge of crystals and their interpretation, lattice dynamics, and the evaluation

of force constants. During this period, IR spectrometry also made tremendous progress and became a more popular and practical analytical technique. From the 1960s, many technological advances resulted, including the lasers, holographic gratings, multichannel detectors, holographic filters, FT-Raman, and computer processing, making Raman spectrometry a very promising technique. A historical summary of Raman spectrometry is shown in Table 1-1.

Comparison of Raman and IR Spectrometry

The basic information of Raman spectrometry is similar to infrared (IR) absorption spectrometry. Both techniques deal with molecular vibrational transitions (rotational transitions information are important for gas phase samples). Usually, for simple molecules, asymmetric modes of vibration are IR active and symmetric modes of vibration are Raman active. If a molecule has a center of symmetry, then the rule of mutual exclusion exists, namely, " fundamentals permitted in IR absorption are forbidden in Raman effect, and fundamentals permitted in the Raman effect are forbidden in IR absorption". However, complex molecules seldom have a center of symmetry and exhibit very few truly symmetrical vibrations that are purely Raman active and IR inactive. Figure 1-1 shows different energy transition schemes among IR, Raman, resonance Raman and fluorescence. In Raman spectrometry, excitation occurs to a virtual state (normal Raman) or electronic state (resonance Raman), then deexcitation to the ground electronic state of different vibrational levels occurs; IR absorption

Table 1-1. Raman spectrometry development timetable.

1923 Smekal first predicted Raman effect theory

1928 C.V. Raman discovered the Raman effect

1934 Placzek predicted the resonance Raman effect phenomenon [7]

1936 The direct photoelectric recording of Raman spectra was invented by Rank and Wiegand [8]

1947 Shorygin observed the first resonance Raman spectrum [9]

1952 Low pressure mercury arc was developed by Welsh et al. [10]

1953 First commercial Raman instruments named Hilger E612 and Cary model 81 [11]

1960 Maiman invented the first laser [12]

1962 Porto and Wood first used a ruby laser as a source for Raman spectrometry [13]

1963 Coherent anti-Stokes Raman scattering was first observed by Terhune. [14]

1964 Landon and Porto employed a two-stage (double) monochromator [15]

1964 Chantry, Gebbie and Hilsum first demonstrated FT-Raman [16]

1970 The charge-coupled device (CCD) was first introduced by Amelio, Thompsett and Smith from Bell lab [17]

1974 Fleischman et al. discovered the surface enhanced Raman effect [18]

1974 The first results of practical Raman microscopy were reported at the IVth International Conference on Raman Spectroscopy in 1974 [19,20]

1986 Jennings, Weber and Brault [21] and Hirschfeld and Chase [22] successfully improved the FT-Raman technique

Figure 1-1. Different transition schemes among IR, Raman, resonance Raman and fluorescence.

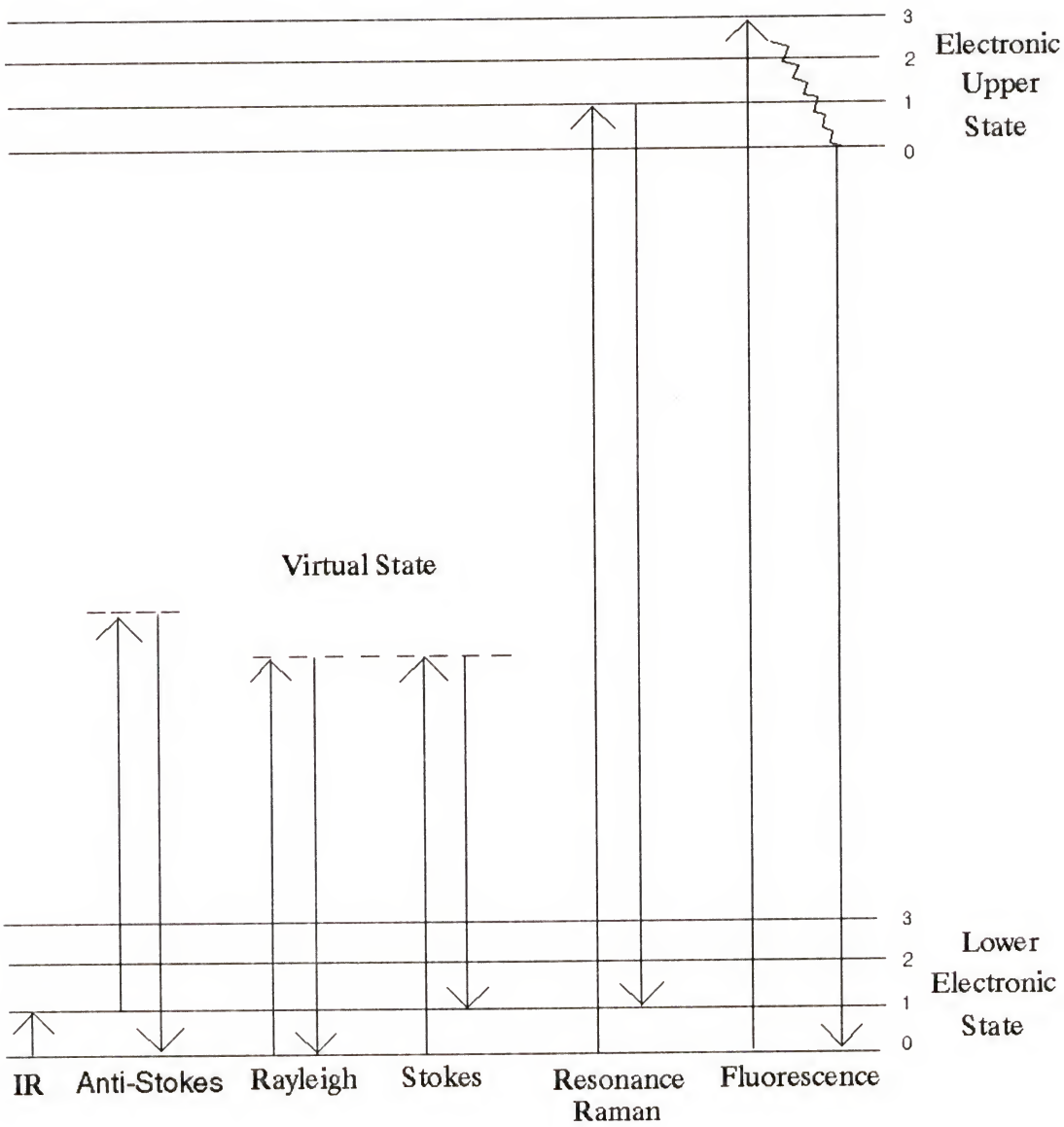

Normal Raman

results in the excitation of different vibrational energy levels in the ground electronic state. Resonance Raman scattering and fluorescence are phenomena which are very often difficult to distinguish. Typically, fluorescence occurs subsequent to the population of an excited state. Prior to emission, this excited state quickly relaxes to the lowest vibrational level of the lowest singlet excited electronic state. Fluorescence emission is broad and relatively long lived in comparison to Raman scattering.

For normal Raman spectrometry, the intensity of Raman peaks depends in a complex way upon the polarizability of the molecule, the intensity of excitation source, and the sample concentration. The Raman scattering bands at wavenumbers less than the incident wavenumber are referred to as Stokes bands, and those at wavenumbers greater than the incident wavenumber as anti-Stokes bands. Figure 1-2 shows an energy-level diagram of Rayleigh and Raman scattering and the resulting Raman spectrum. For resonance Raman, the enhancement of Raman scattering occurs when the excitation wavelength coincides with or is in the region of an electronic absorption band. The cross section of resonance Raman can be two to six orders of magnitude higher than that of normal Raman, but at the same time this visible to ultraviolet excitation light also can produce huge fluorescence signals. Surface-enhanced Raman spectrometry is another technique that allows very small amounts of adsorbates to be investigated with an enhancement of about 10^6 times. For IR spectrometry, the technique deals with the interaction of infrared radiation with matter. The twisting, bending, rotating, and vibrating motions of atoms in a molecule occur simultaneously to produce a highly complex absorption spectrum. The infrared region of the electromagnetic spectrum is

Figure 1-2. (a) Energy-level diagram of Rayleigh and Raman scattering. (b) Part of the resulting spectrum.

(a)

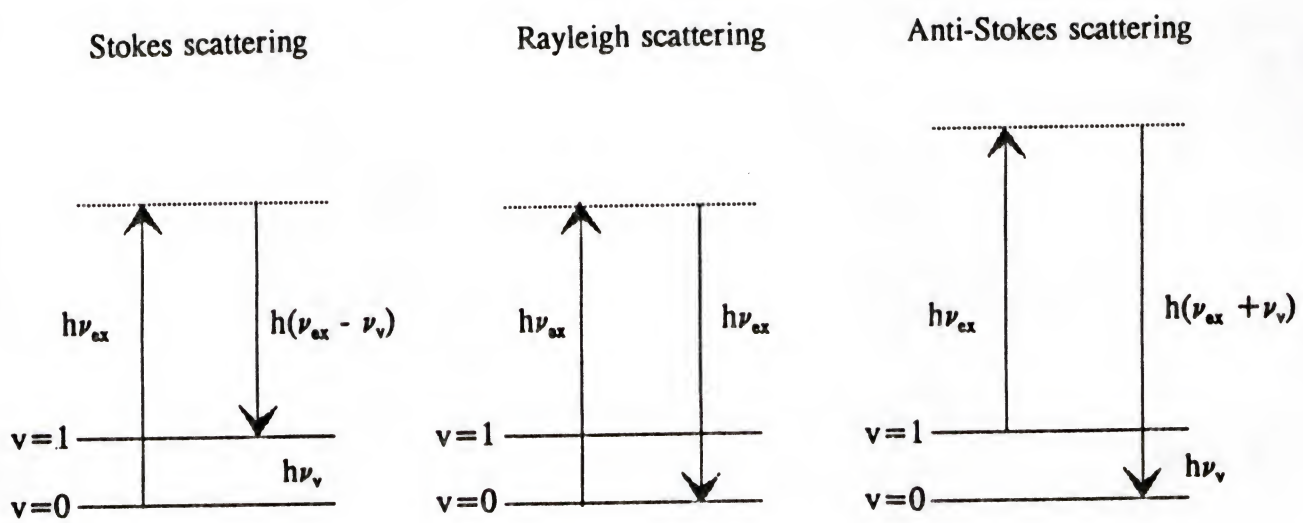
Stokes scattering
Rayleigh scattering
Anti-Stokes scattering
hν_ex
h(ν_ex - ν_v)
v=1
v=0
hν_v
hν_ex
hν_ex
v=1
v=0
hν_ex
h(ν_ex +ν_v)
v=1
v=0
hν_v

(b)

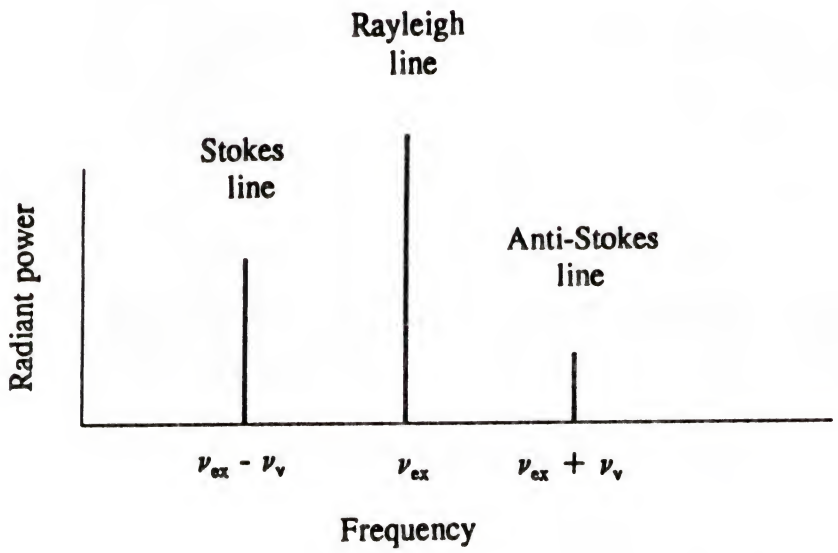
Rayleigh line
Stokes line
Anti-Stokes line
Radiant power
ν_ex - ν_v
ν_ex
ν_ex + ν_v
Frequency

generally considered to liebetween 770 nm and 1000 μm, corresponding to a wavenumber range of 12,900 to 10 cm^{-1}. The IR region is often further subdivided into three subregions. The near-infrared region extends from 770 nm to 2.5 μm (12,900 to 4000 cm^{-1}), the mid-infrared region from 2.5 to 50 μm (4000 to 200 cm^{-1}), and the far-infrared region from 50 to 1000 μm (200 to 10 cm^{-1}).

Although spectra obtained by Raman scattering and IR absorption spectrometry have much in common, there are some differences in the instrumentation and sample handling techniques. A more detailed comparison between Raman and IR spectrometry is shown in Table 1-2.

Intent of Dissertation

The majmr goal of this dissertation work was to develop an incoherent source resonance Raman spectrometer which would be simple, inexpensive, and compact that can be easily used for industrial applications. In this dissertation, the first three chapters give an introduction to Raman spectrometry, popular Raman techniques and focus on the theory, instrumentation and applications of resonance Raman spectrometry. Chapters 4 and 5 will cover the experimental sections on incoherent sources, diagnostical measurements, sample cell designs, experimental conditions, optimization, sample absorption correction and applications. Finally, the last chapter gives discussions and conclusions of experimental results. Possible work in the future will also be discussed.

Table 1-2. Comparison of Raman and IR spectrometry.

	Raman spectrometry	IR spectrometry
Water solvent	good	poor
Cell material	glass or quartz	salts
Detector	1 photomultiplier tube (PMT) 2 photodiode array (PDA) 3 charge-coupled device (CCD) 4 charge-injection device (CID)	1 Golay pneumatic detector 2 triglycine sulfate (TGS) pyroelectric detector 3 mercury-cadmium-telluride photoconductor (MCT) 4 bolometer
Detector response time	fast: good for short-lived or transient species study	slow
Source	laser	Nernst glower
Selection rule	polarizability change	dipole moment change
Depolarization ratio	yes	no
Spectrum	signal weaker, simpler spectrum, less overtone and combination bands	signal stronger, complicated spectrum, sensitive to small structural differences
Popular modes	1 Raman microscopy 2 FT-Raman 3 resonance Raman 4 surface-enhanced Raman 5 coherent anti-Stokes Raman	1 IR microscopy 2 FT-IR 3 internal reflection method 4 attenuated total reflection

CHAPTER 2
ANALYTICAL RAMAN SPECTROMETRY

Introduction

The laser was first used as an excitation source for Raman spectrometry in 1962 by Porto and Wood [13]; this intense and narrow bandwidth light source resulted in a rapid and continuous development of Raman techniques. Although the growth of analytical applications of Raman spectrometry was slower than IR absorption spectrometry, Raman spectrometry techniques became feasible alternatives to IR for structure elucidation, multicomponent qualitative analysis, and quantitative determinations of minor and trace constituents. In this chapter the theory, experimental setup, and different analytical techniques of Raman spectrometry will be discussed.

Theory

Classical Theory

For an incident light, frequency ν_0, in Hz, the electromagnetic wave with a periodically varying intensity of the electric component E can be written

$$E = E_m \cos (2\pi\nu_0 t) \qquad (2.1)$$

where E_m is the amplitude of the electric component, in V m^{-1}, and t is the time, in s.

When a molecule interacts with an electric field it suffers some distortion, with the positively charged nuclei being attracted towards the negative pole of the field, and the electrons to the positive pole. This separation of charges causes an electric dipole moment μ to be induced in the molecule; μ is related to the electric field E of the radiation by the power series [23]

$$\mu = \mu^{(1)} + \mu^{(2)} + \mu^{(3)} + \ldots \tag{2.2}$$

where

$$\mu^{(1)} = \alpha E \tag{2.3}$$

$$\mu^{(2)} = 1/2\ \beta E^2 \tag{2.4}$$

$$\mu^{(3)} = 1/6\ \gamma E^3 \tag{2.5}$$

In these equations, μ and E are vectors with units of C m and V m^{-1}, respectively. Each component of $\mu^{(1)}$ is a different linear combination of the components of E; each component of $\mu^{(2)}$ is a different linear of the components of E^2, and so on. The polarizabilities α, β, and γ are tensors and can be regarded as measures of the ease with which electrons can be displaced to produce an electric dipole under the action of an electric field. Typical orders of magnitude for components of α, β, and γ are as follows: α, 10^{-40} C V^{-1} m^2; β, 10^{-50} C V^{-2} m^3; and γ, 10^{-61} C V^{-3} m^4 [23]. The dipole moment $\mu^{(2)}$ will not be important until the electric field E is higher than 10^9 V m^{-1} (at 10^9 V m^{-1}, $\mu^{(2)}$ is about 1% of $\mu^{(1)}$), and that happens only when focused giant-pulsed laser beams are used to study the nonlinear Raman effect. Because Raman spectrometry is normally used at much lower electric field intensities, the dipole moment μ is given by only the linear

induced dipole moment $\mu^{(1)}$.

The Raman effect results from the interaction of the polarizability with the normal modes of vibration of the molecules. The polarizability varies with internuclear separation around its equilibrium value α_0 and can be presented [24] approximately by

$$\alpha = \alpha_0 + (r - r_e)\,(\partial\alpha/\partial r)_e \tag{2.6}$$

where r is the internuclear separation, in m. The subscript e indicates the equilibrium position. The change in internuclear distance varies periodically during vibration, as indicated by the equation

$$r - r_e = r_m \cos(2\pi\nu_v t) \tag{2.7}$$

where r_m, in m, is the maximum amplitude of the internuclear separation of the molecule of frequency ν_v, in Hz. Substitution of equation 2.7 into 2.6 yields

$$\alpha = \alpha_0 + (\partial\alpha/\partial r)_e\, r_m \cos(2\pi\nu_v t) \tag{2.8}$$

If equations 2.1 and 2.8 are substituted into 2.3, an induced dipole moment can be expressed as μ:

$$\begin{aligned}\mu &= [\alpha_0 + (\partial\alpha/\partial r)_e\, r_m \cos(2\pi\nu_v t)]\,[E_m \cos(2\pi\nu_0 t)] \\ &= \alpha_0 E_m \cos(2\pi\nu_0 t) + E_m r_m (\partial\alpha/\partial r)_e \cos(2\pi\nu_v t)\cos(2\pi\nu_0 t)\end{aligned} \tag{2.9}$$

Trigonometric rearrangement of $\cos x \cdot \cos y = 1/2 \cos(x-y) + 1/2 \cos(x+y)$ into equation 2.9 gives

$$\begin{aligned}\mu = \alpha_0 E_m \cos(2\pi\nu_0 t) &+ 1/2\, E_m r_m (\partial\alpha/\partial r)_e \cos 2\pi(\nu_0 - \nu_v)t \\ &+ 1/2\, E_m r_m (\partial\alpha/\partial r)_e \cos 2\pi(\nu_0 + \nu_v)t\end{aligned} \tag{2.10}$$

The equation 2.10 represents the three major phenomena observed in a simple Raman spectrometry experiment. The first term is a result of elastic scattering, known as the

Rayleigh scattering, while the second and third terms are a result of inelastic scattering involving Stokes and anti-Stokes Raman scattering. For Raman scattering to occur,

$$(\partial\alpha/\partial r)_e \neq 0. \tag{2.11}$$

This means polarization must change during a vibration if that vibration is to be Raman active.

Polarizability and Depolarization Ratio

The polarizability α is a tensor and has components in each of the x, y, z directions of a Cartesian coordinate system. As a result, equation 2.3 of the induced dipole moment may be expressed as

$$\begin{aligned} \mu_x &= \alpha_{xx}E_x + \alpha_{xy}E_y + \alpha_{xz}E_z \\ \mu_y &= \alpha_{yx}E_y + \alpha_{yy}E_y + \alpha_{yz}E_z \\ \mu_z &= \alpha_{zx}E_z + \alpha_{zy}E_y + \alpha_{zz}E_z \end{aligned} \tag{2.12}$$

Because $\alpha_{ij} = \alpha_{ji}$, the number of distinct components of the tensor is reduced from nine to six. There are two invariant (constant regardless of the orientation of the molecule) properties of the polarizability tensor which are referred to as the mean polarizability $\bar{\alpha}$ and anisotropy γ, which are given by

$$3\bar{\alpha} = \alpha_{xx} + \alpha_{yy} + \alpha_{zz} \tag{2.13}$$

$$2\gamma^2 = (\alpha_{xx} - \alpha_{yy})^2 + (\alpha_{yy} - \alpha_{zz})^2 + (\alpha_{zz} - \alpha_{xx})^2 + 6(\alpha_{xy} + \alpha_{yz} + \alpha_{zx}) \tag{2.14}$$

One consequence of the polarizability tensor being symmetrical is that spontaneously scattered light with directional properties is produced. These can be expressed in terms of an average scattering tensor for an assembly of randomly oriented tumbling molecules assuming the assembly contains only the invariant parts of the individual molecular

polarizability tensors. The average values of the square of the tensor elements (averaged over all orientations) can be expressed as

$$\overline{\alpha}^2_{ii} = \overline{\alpha}^2_{xx} = \overline{\alpha}^2_{yy} = \overline{\alpha}^2_{zz} = (45\overline{\alpha}^2 + 4\gamma^2)/45 \tag{2.15}$$

$$\overline{\alpha}^2_{ij} = \overline{\alpha}^2_{xy} = \overline{\alpha}^2_{yz} = \overline{\alpha}^2_{zx} = \gamma^2/15. \tag{2.16}$$

When the incident beam is polarized, the Raman scattered radiation can be polarized to various degrees depending on the nature of the active vibration. The depolarization ratio, ρ, is defined as the anisotropic scatter (which is governed by the $\overline{\alpha}^2_{ij}$) over the isotropic scatter (which is governed by $\overline{\alpha}^2_{ii}$) and is given by

$$\rho = \frac{\overline{\alpha}^2_{ij}}{\overline{\alpha}^2_{ii}} = \frac{3\gamma^2}{45\overline{\alpha}^2 + 4\gamma^2} \tag{2.17a}$$

and ρ also can be measured by

$$\rho = \frac{(\Phi_R)_\perp}{(\Phi_R)_\parallel} \tag{2.17b}$$

where $(\Phi_R)_\perp$ is the Raman radiant power polarized perpendicular to the original beam and $(\Phi_R)_\parallel$ is the Raman radiant power polarized parallel to the original beam.

The depolarization ratio can give information about the symmetry of the vibration involved. In the case of a molecule with spherical symmetry and a totally symmetric vibration, ρ is equal to zero. On the other hand, if the vibration distorts the symmetry, or if the molecule is not symmetric to begin with, a significant depolarization ratio up to 0.75 can occur.

Raman Intensities

In the early 1930s, Placzek [7] developed a polarization theory that allowed the formulation of equations determining the experimentally observed intensities of the Raman Stokes and Raman anti-Stokes scattering. The basic assumptions required that the excitation frequency ν_0 be much higher than the vibration transition ν_v but much smaller than the electric transition ν_e. The radiant power of the Stokes, $\Phi_{R(St)}$, and anti-Stokes, $\Phi_{R(aSt)}$, Raman bands has been derived by Placzek [7], assuming observation of the scattered radiation at an angle of 90° to the exciting beam.

$$\Phi_{R(St)} = \frac{2\pi^2 h}{c} \frac{(\bar{\nu}_o - \bar{\nu}_v)^4}{\bar{\nu}_v[1 - \exp(-hc\bar{\nu}_v / kT)]} g_v \left(\frac{\partial \alpha}{\partial r}\right)_e^2 \qquad (2.18)$$

$$\Phi_{R(aSt)} = \frac{2\pi^2 h}{c} \frac{(\bar{\nu}_o + \bar{\nu}_v)^4}{\bar{\nu}_v[\exp(hc\bar{\nu}_v / kT) - 1]} g_v \left(\frac{\partial \alpha}{\partial r}\right)_e^2 \qquad (2.19)$$

where h is the Planck constant, in J s, k is the Boltzmann constant, in J K^{-1}, T is the absolute temperature, in K, $\bar{\nu}_o$ and $\bar{\nu}_v$ are wavenumbers (cm^{-1}) corresponding to the frequencies of the exciting radiation and molecular vibration, and g_v is degeneracy of the given vibration of the molecule. From equations 2.19 and 2.18, the anti-Stokes to Stokes radiant power ratio shows a dependence on the absolute temperature of the sample, which can be expressed as

$$\frac{\Phi_{R(aSt)}}{\Phi_{R(St)}} = \frac{(\bar{\nu}_o + \bar{\nu}_v)^4}{(\bar{\nu}_o - \bar{\nu}_v)^4} e^{-hc\bar{\nu}_v/kT} \qquad (2.20)$$

Instrumentation

A Raman spectrometer normally consists of an intense source, a sample cell, wavelength selection devices, and a detector.

Sources

Discharge lamps. Before the laser was introduced to Raman spectrometry in 1962, discharge lamps were the primary source for Raman spectrometry. However, the mercury arc was almost the only practical discharge lamp of monochromatic radiation source for the excitation of Raman spectra. The typical power emitted by a 2.5 kW Toronto mercury arc at Hg e (435.8 nm) line into a 4π sr solid angle is about 50 W; because of the divergence of the radiation, only about 1 W can be collected within the sample and used for excitation [25]. The most intense lines provided by the mercury-arc lamp are 253.7 (resonance line), 404.6, 435.8, and 546.1 nm.

Laser sources. The first popular laser-excited Raman source was the He-Ne laser, which operates in a continuous mode at a power of 50 mW. Laser radiation is produced at 632.8 nm. However, most applications of Raman spectrometry have involved using the powerful (e.g., >1W) argon ion laser with intense spectral output at the 488.0 nm or 514.5 nm. Since the intensity of Raman scattering varies as the fourth power of the

frequency of the exciting source, Ar^+ lasers can provide a significant improvement in Raman intensity over the He-Ne laser. In addition, the most commonly used detectors have higher responsivities in the blue or green than in the red.

Another source that has been used in analytical Raman spectrometry is the pulsed Nd/YAG laser. It is a solid-state device offering reliability and power of operation. It can be used for FT-Raman spectrometry, at 1064 nm, or normal Raman spectrometry, at frequency-doubled 532 nm, or resonance Raman spectrometry by nonlinear frequency doubling, with mixing of the pumped dye laser output at the UV wavelength region.

Diode lasers have made dramatic strides in the last few years and are now available with reasonable power levels (up to 300 mW) in the 600 nm and 1000 nm range [26]. These lasers operate in the near infrared region where most molecular fluorescence interference is eliminated. The red-extended CCD detectors, coupled with the diode lasers, have made a good combination for multichannel Raman spectrometers and FT-Raman spectrometers.

Sample Cells

Raman spectra can be readily obtained with gas, liquid, and solid samples. Sample handling for Raman studies tends to be simpler than for infrared, because the scattered radiation is in the near IR to UV region and cell materials, windows, and optical materials can be made of glass or quartz. Since the excitation beam is very intense, flow cells (liquids and gases) and rotating sample holders are popularly designed to avoid overheating the sample.

The scattered radiation is commonly viewed at 90^0 to the direction of the exciting beam, thus minimizing scatter interference from the primary beam. The intensity of Rayleigh scattering is then about 0.1% of the exciting beam intensity, and the Raman scattering intensity is about 10^{-5}% lower [27]. If the sample is transparent to the laser beam, two concave mirrors can be added to the sample cell system to increase the scattered Raman radiation about fourfold from that obtainable without the mirrors. Two possible arrangements for Raman scattering observation at 90^o are shown in Figure 2-1a and 2-1b.

Observation of backscattered radiation may be useful in sample-surface examination and high absorption resonance samples (Fig 2-1c); however, 180^o illumination / observation is normally used in surface-enhanced Raman spectrometry. In resonance Raman spectrometry, $\sim 135^o$ is a better choice to minimize the strong specular reflection from the sample surface.

Gas-phase samples have relatively small concentrations of analyte molecules and require higher-powered lasers and a more complicated sampling system than liquid samples. A multiple reflection cell is often used to increase the path length by passing the excitation light several times through the sample cell, as shown in Figure 2-1d.

Wavelength Selection Devices

Filters. Since the laser is usually not a pure monochromatic source, a line filter is used before the illuminated sample cell. It is normally either a narrow band pass interference filter or a prism monochromator. Requirements for an effective filter are a high degree of transmission at the laser line and adequate rejection at other

Figure 2-1. Examples of different sample cells and Raman scattering observation arrangements. (a) Solution in a tube observed at 90^0. (b) Transparent sample with two concave mirrors to increase the scattered radiation. (c) Sample observed at 180^0. (d) Multipass cells for gas phase.

(a)

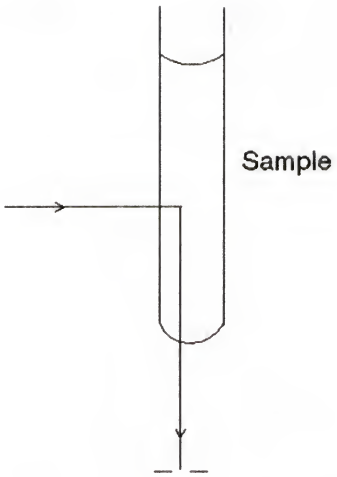

(c)

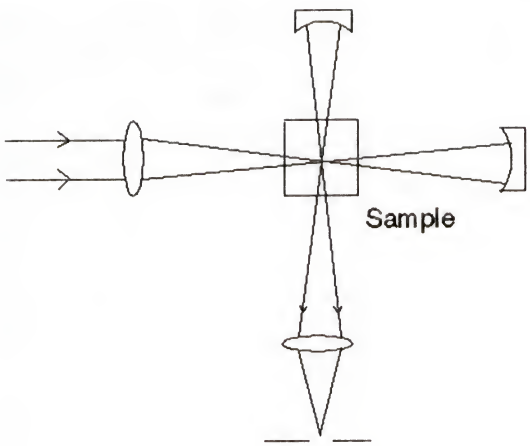

(b)

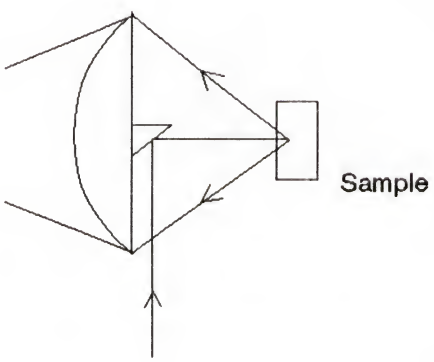

(d)

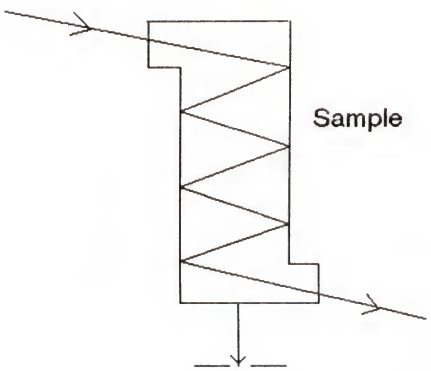

wavelengths. This rejection filter reduces nonlasing emission lines that are present and are elastically scattered by the sample producing artifacts in the Raman spectrum.

Another kind of filter which reduces the Rayleigh light from the sample scattering is the holographic filter. These multilayer dielectric devices have high transmission (80% or better) over a wide frequency range, and extinction at the laser line which can be as high as 5 to 6 optical density units [28,29]. Holographic filters are angle tunable and as a result, angle sensitive. They operate best in a collimated beam and are commercially available from the near IR to visible region.

Monochromators. Conventional Raman spectrometers are usually provided with a monochromator in which the radiation is dispersed by diffraction gratings. The replacement of ruled gratings with holographic gratings in modern spectrometers has led to significant improvements in stray radiation rejection. The use of monochromators with two or three gratings also increases the resolving power of the spectrometer and reduces the background caused by Rayleigh scattering in the sample. However, the more gratings a monochromator uses the lower the throughput. The new development in this area is the rapid development of single monochromators for Raman spectrometry with good cut-off filters, such as holographic filters, to remove most of the Rayleigh scattering. Single monochromators can function as dispersing units with high throughput.

Detectors

Photographic detection was used before photomultiplier tubes (PMT) became popular. The advent of the PMT caused a resurgence of interest in Raman spectrometry because of its relatively sensitive, low-noise character. Photons incident on the

photocathode cause emission of electrons, the number emitted being proportional to that of the number of photons. However, a photocathode will also emit thermoionic electrons, which on passing to the anode produce a background for the photoelectrons. The current produced by these thermoionic electrons is called the dark current, which can be reduced by cooling the photomultiplier tube.

Recent technological advancements have resulted in several new types of multichannel ultraviolet and visible light detectors. Two classes of these detectors which are currently available are photodiode arrays (PDAs) and charge-coupled devices (CCDs).

Photodiode arrays [30], PDAs, have been used in spectroscopic applications for more than ten years to record spectrally dispersed light from monochromators. Although the signal-to-noise ratio (S/N) of a typical photodiode array is lower than that of a PMT, adequate Raman signals can be obtained when a high power laser is used with PDAs.

Charge-coupled devices have been used extensively in the last few years owing to their low noise characteristics, two-dimensional multichannel capability, and high quantum efficiency. Moreover, the low cost and versatile software packages make manipulation and analysis of the acquired data more convenient.

Analytical Techniques of Raman Spectrometry

The analytical techniques of Raman spectrometry continue to grow as mature analytical tools although the techniques are still not as widely used in industrial analysis

owing to the speed, accuracy, and cost compared to infrared spectrometry. Yet there are many situations in which Raman spectrometry is the preferred method over infrared spectrometry because of its capability to study systems *in situ* under nonambient conditions, to obtain high degree of spatial resolution offered by the Raman microprobe, and to work in aqueous solutions.

Raman Microscopy

Raman microscopy is an instrument that couples a Raman spectrometer with an optical microscope, allowing the examination of a surface down to 1 μm. A typical Raman microscope system is shown in Figure 2-2. A TEM_{00} visible laser beam from either an argon or krypton ion laser or dye laser is directed into a beamsplitter. A portion of the incident laser radiation is reflected downwards by the beamsplitter and a portion of light is transmitted through the beamsplitter. The reflected beam passes through the microscope objective lens, which serves to focus the laser beam to a diffraction limited spot on the sample and to collect the scattered radiation from the sample. This scattered radiation is transmitted through the beamsplitter to be viewed on the viewing screen or directed by a prism and coupling optics to the entrance slit of the monochromator. The Raman signal is then detected either by the cooled PMT or the multichannel detector.

Raman microscopy is a significant development for examining molecular species on surfaces. Raman microscopy has been applied to polymers, films, fibers, biological specimens, semiconductors, and environmental pollution studies. The most rapidly expanding area of application of Raman microscopy is the spatially resolved study of

Figure 2-2. Schematic of a typical Raman microscope system.

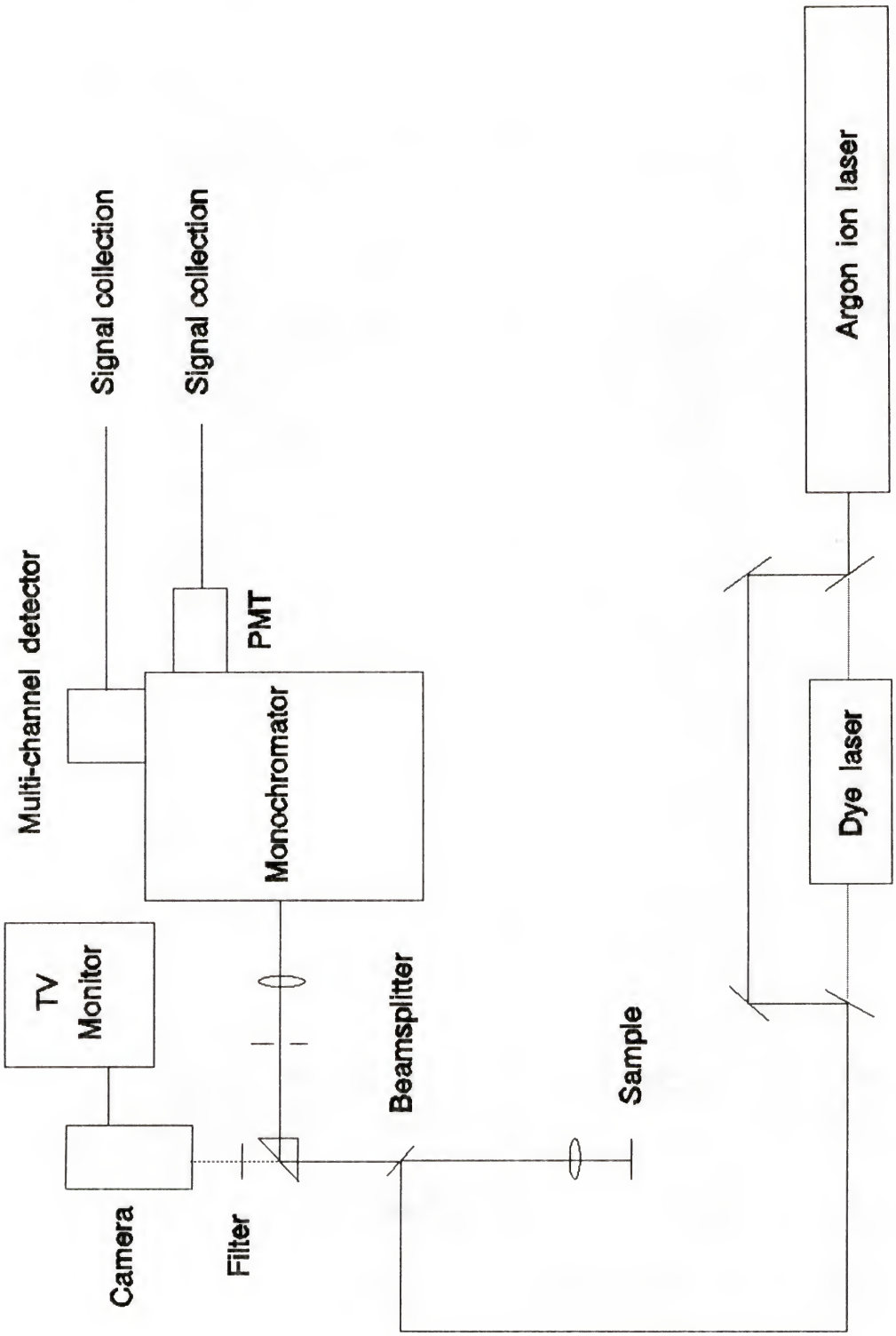
Argon ion laser
Dye laser
Sample
Beamsplitter
Filter
Camera
TV Monitor
Monochromator
PMT
Multi-channel detector
Signal collection
Signal collection

geological materials, particularly in the characterization of fluid inclusions [31].

Fourier Transform Raman Spectrometry

Near IR Fourier transform (FT) Raman spectrometry has successfully reduced fluorescence and thermal decomposition problems of Raman spectrometry. In addition, FT measurements use Michelson interferometers, which have both multiplex and throughput advantages when compared with conventional grating instruments. However, the major problem of FT Raman is the strong scattered laser radiation, which can completely fill up the dynamic range of the A/D converter and detection system or force the detector into a nonlinear response region. Several types of filters, such as multistage interference filters and very high rejection ratio filters, called Chevron filters, have been used to achieve rejection ratios on the order of 10^{-9} to 10^{-10} [32]. In this case, FT-Raman measurements, in the near-IR region, provide S/N values in the range 10^2 to 10^4, which is in the same range as ordinary Raman measurements. A optical diagram of an FT-Raman spectrometer is shown in Figure 2-3.

Resonance Raman Spectrometry

When Raman scattering is excited by radiation with a frequency near or coincident with an electronic absorption peak of the analyte, it is referred to as resonance Raman spectrometry. The enhanced resonance Raman bands have intensities 10^2 - 10^6 times greater than normal Raman intensities. Consequently, resonance Raman spectra have low detection limits and are much simpler than normal Raman spectra, since only bands related to the chromophore are enhanced. More details of resonance Raman spectrometry will be discussed in the next chapter.

Surface-Enhanced Raman Spectrometry

In 1974, Fleischmann, Hendra, and McQuillan [18] reported very intense bands from pyridine adsorbed on an anodized silver surface. These Raman enhancements ($\sim 10^6$ x) were later observed for a variety of adsorbates on several metal surfaces; the resulting Raman process is called surface-enhanced Raman scattering (SERS).

One of the major considerations for the formation of a SERS surface is surface roughness; surface roughness has been achieved in various ways. Vo-Dinh and co-workers [33] have shown that SERS effects can be achieved from silver-coated spheres ranging from 38 to 1000 nm in diameter. The theories for surface enhancement could be divided into two classes: the chemical enhancement mechanisms, in which α is perturbed by interactions of the adsorbates with the surface, and electric field enhancement mechanisms, in which the field experienced by the molecule is greater than it would experience without the presence of the surface [34]. Four strongly enhanced metals substrates are silver, gold, copper, and nickel. For silver surfaces, green laser light (typically 514.5 nm) is the best, whereas for copper and gold the lower-energy laser lines (e.g., 647.1 nm) give better results. However, the overall frequency dependence is a complex function of surface roughness and substrate dielectric properties.

Surface-enhanced resonance Raman spectrometry (SERRS) occurs when the laser excitation wavelength is coincident with an absorption band in the adsorbate. Surface-enhanced resonance Raman scattering can further enhance the Raman scattering efficiency by factors of 10^3 to 10^5 times above the enhancement observed under either resonance enhanced or surface-enhanced conditions [35].

Figure 2-3. Optical diagram of an FT-Raman spectrometer.

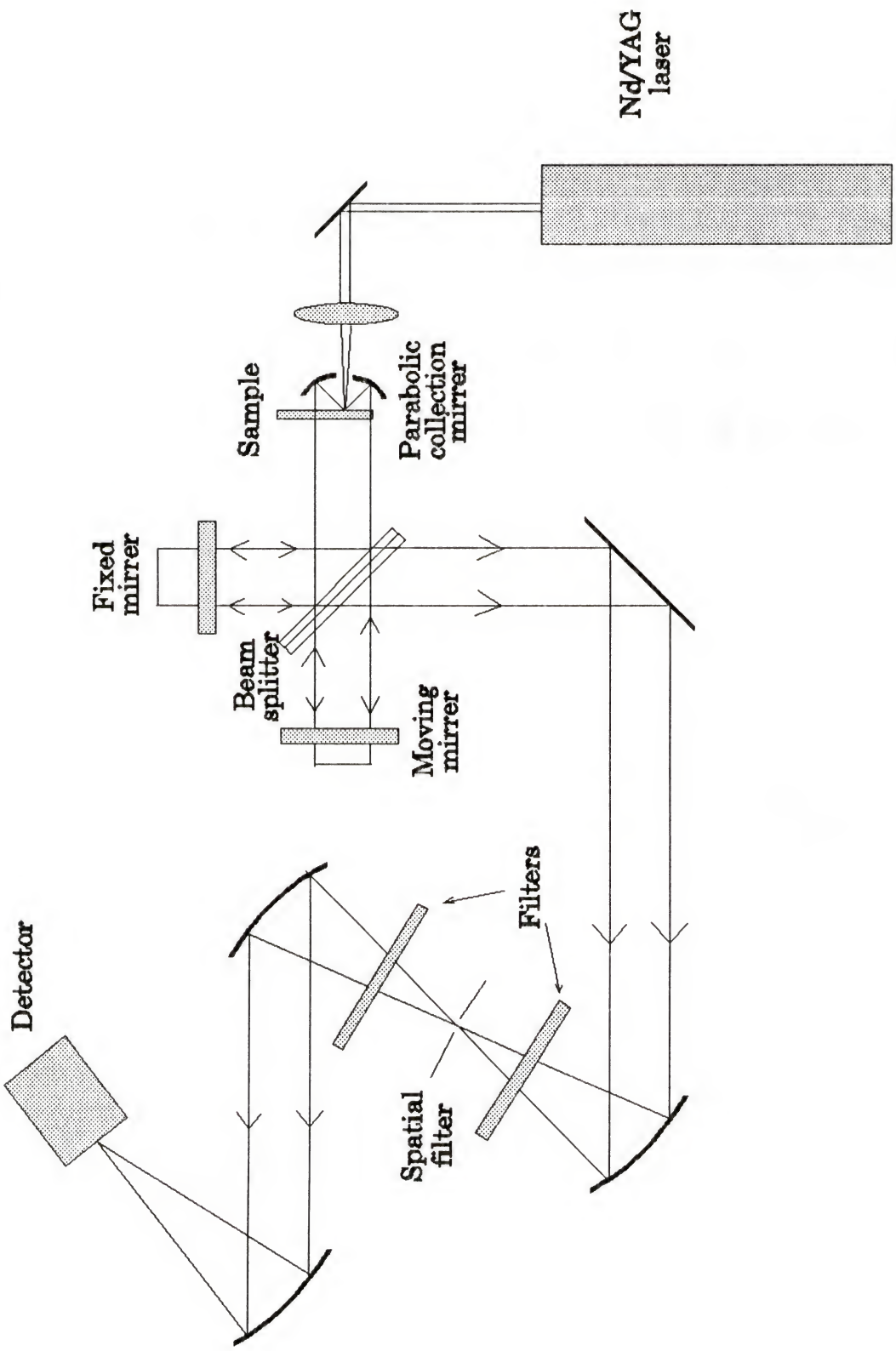
Nd/YAG laser
Parabolic collection mirrer
Sample
Fixed mirrer
Beam splitter
Moving mirrer
Filters
Spatial filter
Detector

Coherent Anti-Stokes Raman Spectrometry

Coherent anti-Stokes Raman spectrometry (CARS) is a popular nonlinear Raman spectrometry method because the signal is in the anti-Stokes region, where it can be spectrally and spatially distinguished from fluorescence. The Raman spectrum can be observed at high laser irradiances with electric field strengths over about 10^9 Vm^{-1}. As illustrated in Figure 2-4, CARS is a three-wave technique which uses two laser sources, a pump beam at ν_l and a Stokes shifted probe beam at ν_s. If these two beams are focused into the sample at sufficient power and with suitable phase matching conditions, a third beam of frequency $\nu_a = 2\nu_l - \nu_s$ is generated. The probe beam, normally from a tunable laser, is scanned to generate the third frequency continuously. The power generated at this third frequency is normally very weak until the pump and probe frequencies differ by the frequency of a vibrational transition. At present, CARS is still a relatively expensive technique and has found its major analytical application in gas-phase spectrometry, particularly for the study of combustion and in studies of strongly fluorescent biological compounds separated by HPLC.

Figure 2-4. (a) Energy-level diagram illustrating the CARS process. ν_l: laser frequency, ν_s: Stokes (probe beam) frequency, ν_a: anti-Stokes frequency. (b) CARS scattering phase-match diagram. k_l, k_s, and k_a: wave vectors of ν_l, ν_s, and ν_a.

(a)

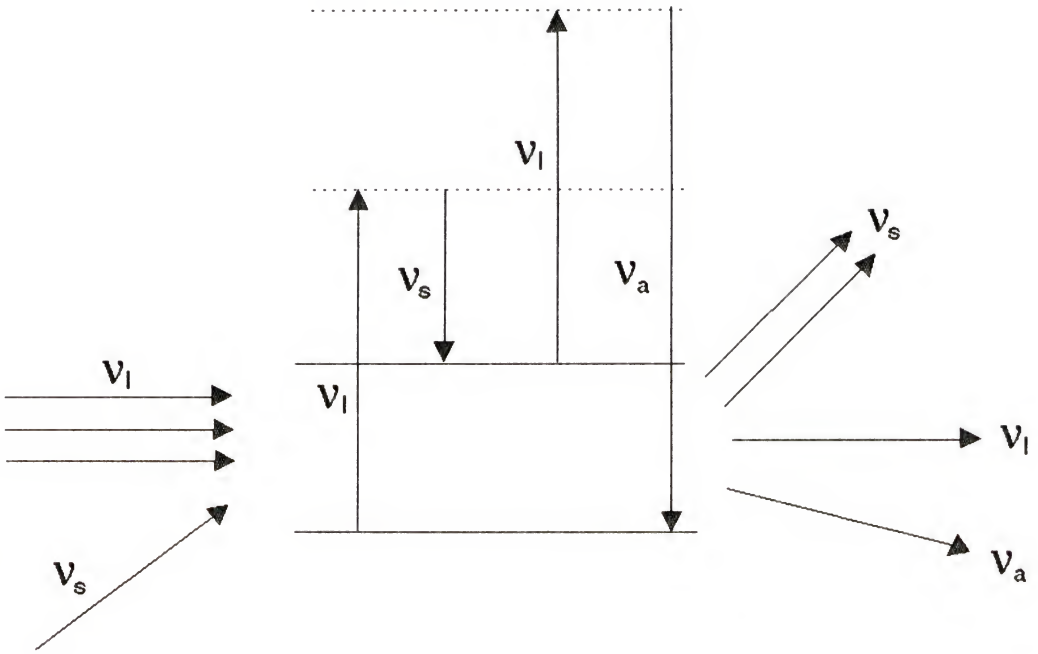

(b)

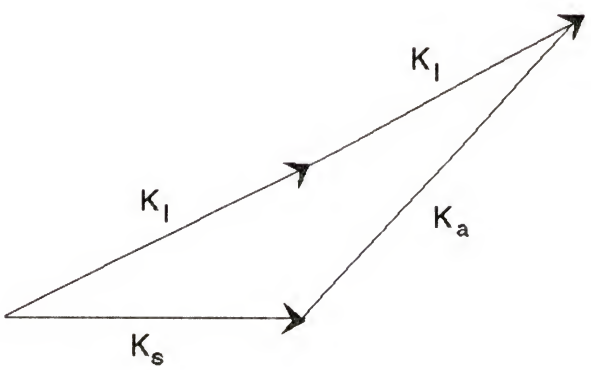

CHAPTER 3
RESONANCE RAMAN SPECTROMETRY

The rapid development of new experimental techniques, in particular highly efficient lasers, monochromators, filters, and detection systems, has made resonance Raman spectrometry a promising technique in the future. Theories describing the intensity of the resonance Raman effect have been reviewed in several papers [36-42]. For this chapter, several important topics for resonance Raman spectrometry, such as basic theory, instrumentation, and applications, will be covered.

Theory

The resonance Raman effect can substantially improve the selectivity of Raman measurements on complex molecules. The selective resonance enhancement of particular vibrations and the Raman excitation profile data can be understood by considering the theory of resonance Raman intensity. Suppose a molecule, initially in a vibronic state m, is excited by incident light of frequency ν_0 , in Hz, and intensity I_0, in W sr^{-1}, in a manner causing it to pass into a vibronic state n while scattering light of frequency $\nu_0 \pm \nu_{mn}$. The total Raman intensity I_{mn}, in W sr^{-1}, scattered over the solid angle 4π sr by randomly oriented molecules is given by the expression [43]

$$I_{mn} = \frac{2^7\pi^5}{3^2c^4} I_0 |\sum_{\rho\sigma} (\alpha_{\rho\sigma})_{mn}|^2 (\nu_0 \pm \nu_{mn})^4 \qquad (3.1)$$

where c, in m s^{-1}, is the velocity of light and the sum goes over ρ=x,y,z and σ=x,y,z which independently refer to the molecule's fixed coordinate system.

The component $\alpha_{\rho\sigma}$ of polarizability tensor can be calculated by the interaction of the molecule and the incident-radiation field. The reason for the enhancement can be seen from the following expression

$$(\alpha_{\rho\sigma})_{mn} = \frac{1}{h}\sum_e [\frac{(M_\rho)_{en}(M_\sigma)_{me}}{\nu_{em} - \nu_0 + i\Gamma_e} + \frac{(M_\rho)_{me}(M_\sigma)_{en}}{\nu_{en} + \nu_0 + i\Gamma_e}] \qquad (3.2)$$

where h, in J s, is the Planck constant, ν_{em}, ν_{en}, in Hz, are the frequency obtained from the energy differences of the vibronic states, and $i\Gamma_e$,in Hz, is a damping term related to the width of the excited state ν_e (the bandwidth of the electronic transition). Here $(M_\rho)_{en}$, $(M_\sigma)_{me}$ refer to the amplitudes of the corresponding transition moments. Thus, for example, $(M_\rho)_{en}$ represents the amplitude of the transition moment

$$(M_\rho)_{en} = \int \Psi_n^* m_\rho \Psi_e d\tau \qquad (3.3)$$

where Ψ_e and Ψ_n are the vibronic wave functions and m_ρ is the ρth component of the electric moment operator. The first term of the equation 3-2 is the resonant term. When the incident laser frequency ν_0 is chosen near the excited electronic transition ν_{em}, the denominator, $(\nu_{em} - \nu_0 + i\Gamma_e)$, of the resonant term becomes very small, so that the polarizability element becomes very large. This effect is called the resonance Raman

effect, which can effectly increase the Raman cross section by two to six orders of magnitude.

The preresonance Raman spectra can be obtained with an excitation source at a frequency just slightly lower than that necessary to cause an electronic transition. The spectra can be slightly enhanced (often less than 10-fold).

Instrumentation

The instrumentation of Raman spectrometry has been reviewed in the chapter 2. In this section, more specific instrumental designs for resonance Raman spectrometers will be discussed, especially, the UV resonance Raman system which can reduce fluorescence background and increase the Raman scattering signal.

For resonance Raman spectrometry, the most important requirements for such equipment are (1) an easily tunable excitation source (either in steps or continuously) that covers wavelengths from the visible to the far-UV region; (2) the linewidth of the exciting line should be as small as possible; approximate monochromaticity is necessary for good resolution, particularly for rotational (pure rotational and vibrational-rotation) resonance Raman spectrometry; (3) the exciting beam should be as collimated and intense as possible; these properties are needed to reduce absorption losses of the scattered light in the sample; (4) the analyzer (monochromator plus detector) should be as sensitive and highly resolving as possible.

Excitation Sources

Resonance Raman excitation laser systems have been used by several research groups (Figure 3-1). Asher and coworkers [44] used a Nd-YAG laser which was frequency-doubled or -tripled to pump a dye laser system. By nonlinear frequency doubling and mixing of the dye laser output or doubled output with the 1.06-μm YAG fundamental, continuously tunable light between 200 nm to 750 nm was generated. Hudson [45] combined a Nd-YAG laser with a hydrogen gas Raman shifting cell. This system could provide 14 different wavelengths between 184 nm to 266 nm by mixing different harmonics of the Nd-YAG laser with 1,2,3, and 4 intervals of the 4155 cm^{-1} vibration of hydrogen. The Nd-YAG laser system normally has a low repetition rate (20 Hz) with $\sim$5 ns frequency pulses which has a low duty cycle of about 10^{-7}. This represents a major limitation because an average power of 20 mW corresponds to a peak power level of $\sim$200 kW. A power flux value of 2.5 GW/cm^2 would occur if this beam were focused into a 100-μm-diameter spot size. These short-pulsed laser sources can induce nonlinear optical phenomena in matter, sample decomposition, and saturation problems [46]. A solution to this low duty cycle is to use a higher repetition rate excimer laser. Lin et al. [47] used an injection-locked KrF excimer laser, providing radiation at 249 nm with narrow and low divergence. Asher's group [48] combined a XeCl excimer laser with a dye laser and doubling frequency technique to generate light between 206 nm to 950 nm.

Recently, an intracavity-doubled CW Ar^+ laser has been developed which generates many discrete lines between 229- 529 nm with powers of tens to two

Figure 3-1. Different laser excitation source systems for resonance Raman spectrometry.

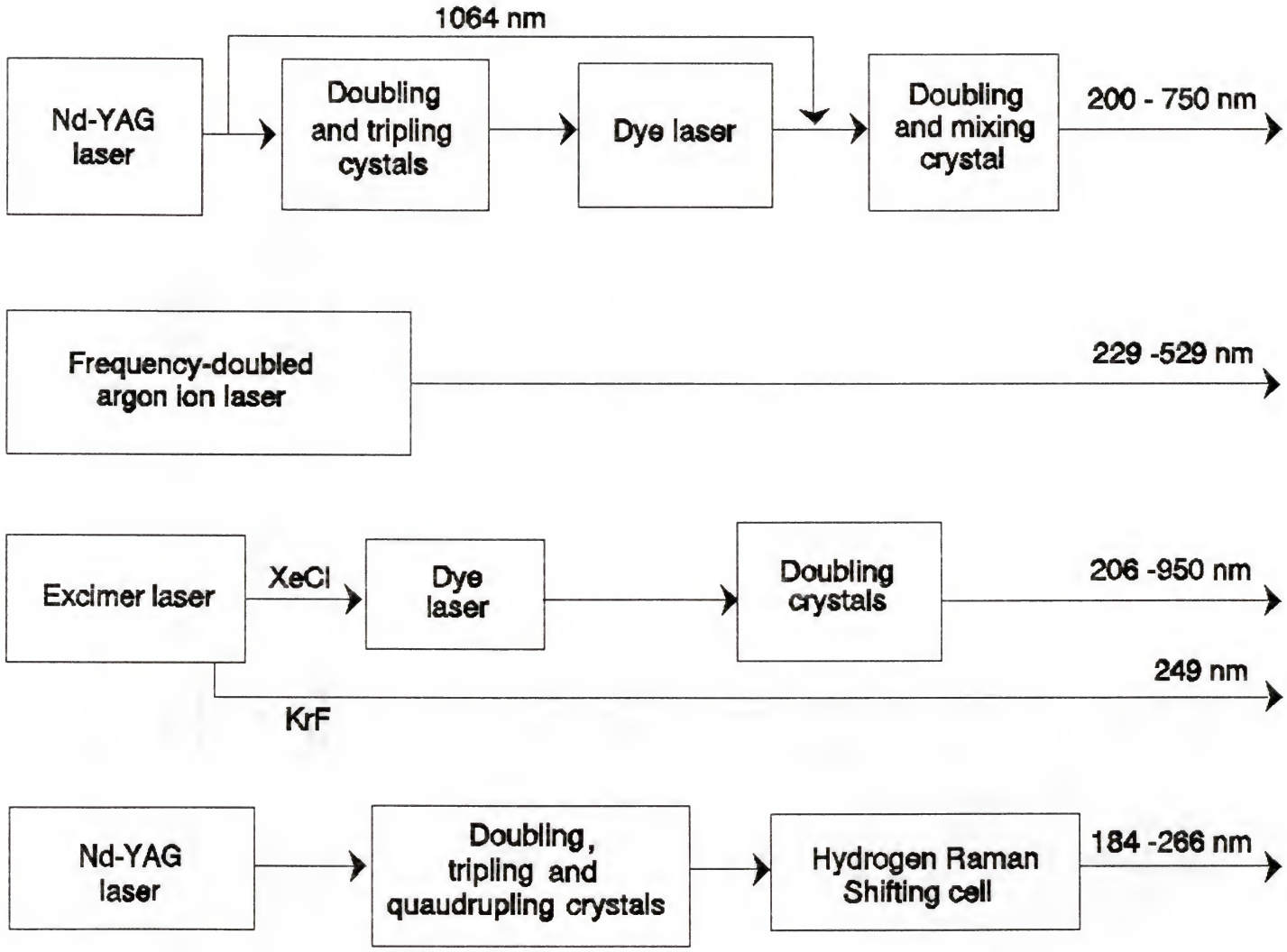
1064 nm
Nd-YAG laser
Doubling and tripling cystals
Dye laser
Doubling and mixing crystal
200 - 750 nm
Frequency-doubled argon ion laser
229 -529 nm
Excimer laser
XeCl
Dye laser
Doubling crystals
206 -950 nm
249 nm
KrF
Nd-YAG laser
Doubling, tripling and quaudrupling crystals
Hydrogen Raman Shifting cell
184 -266 nm

thousand mW. This laser has been shown to be a better choice for resonance Raman spectrometry [46].

Sample Handling and Collecting Optics

Resonance Raman sampling normally requires flowing (liquid and gas phase) or rotating (solid phase) the sample through the laser beam. With a pulsed laser, it is essential to exchange each illuminated sample volume before the arrival of the next laser pulse to avoid sample overheating; also, the high energy UV photons might cause photochemical degradation in the sample.

The collection optics can be either an ellipsoidal mirror or quartz or glass lenses. Either backscattering or 90^0 geometry may be used. Backscattering has the distinct advantage that the Raman scattered intensity does not depend critically on the optical density of the sample. Scattering somewhat off 180^0 has the additional advantage that reflected excitation light is not directed back toward the entrance slit.

Spectrometer and Detection Systems

The spectrometer systems typically used for resonance Raman spectrometry fall into two categories. Either a complex spectrometer (e.g., triple monochromator) is used to obtain a good Rayleigh light rejection but low throughput efficiency or a single long pathlength monochromator combined with a well designed filter is used to obtain a high throughput efficiency but has poor dispersion. Also, with the latter case, limited filters are available for the UV region. The detection device for scanning spectrometers is a photomultiplier tube which is relatively inexpensive; however, only a small fraction of the spectrum is examined at any time and the signal-to-noise ratio is not generally

shot-noise limited. Most of the noise often results from the poor stability of the laser source. For multichannel detector devices, a large fraction of the Raman spectrum is simultaneously accumulated, which normalizes pulse-to-pulse fluctuations. Multichannel detectors, such as charge-coupled devices, have high sensitivities and low noise levels and have become the major detector device for the resonance Raman spectrometer.

Applications

Biological Applications

Raman spectrometry has become an important technique for obtaining structural information on biological systems, primary as a result of the small sample volumes and the use of aqueous solutions. Because of the poor detection limits of conventional Raman spectrometry, resonance Raman spectrometry has become an important technique. There are a number of excellent reviews [38,42,49] about resonance Raman spectrometry that show its usefulness in biological areas. Resonance Raman spectrometry is particularly useful for biological applications since the nature of the effect is such that only the modes associated with the chromophoric group of a molecule are enhanced. The consequences of this are (1) vibrational modes of chromophoric groups in biological molecules, which are often the sites of the biological activities, will be strongly enhanced; (2) the remainder of the vibrational modes will not be enhanced and therefore, cannot complicate the spectrum. Resonance Raman spectrometry has been used as a probe for structural inhomogeneities in the heme protein [50] and has been used for obtaining Raman spectra

of transient intermediates in protein ligand binding [51]. The use of resonance Raman spectrometry to probe protein structure and dynamics has been reviewed [52]; membrane protein has been studied by ultraviolet resonance techniques, an area where biological groups have found several useful applications of ultraviolet excitation [38].

Polymer Applications

Raman spectrometry has some distinct advantages over other techniques for the study of polymer structures. Unlike many other analytical techniques, Raman spectrometry can be applied without sample preparation. It is nonintrusive and usually nondestructive. It can be used easily to study small samples and surfaces, and is high in information content. The developments and applications of Raman spectrometry of polymers have been reviewed by Koenig [53] and Gerrard and Maddams [54].

The biggest limitation to its application has been fluorescence, often coming from fillers, traces of catalyst, monomers, other impurities, or in some cases from the polymer itself. One of the most effective means of avoiding fluorescence interference is through the use of UV excitation at wavelengths shorter than 250 nm.

Resonance Raman spectra of low concentrations of unsaturated species in polypropylene samples, by exciting thin sheet samples at 220 nm, have been reported by Asher's group [55]. The opportunities and problems likely to be encountered through the use of UV excitation for both conventional Raman spectra in UV-transparent polymers and resonance Raman spectra have been elucidated by Chadha, et al.[56]. Williams and Klenerman [57] have also recently applied Raman spectrometry to analytical problems of petroleum samples and polymers.

Inorganic Applications

The Raman technique is often superior to IR absorption for investigating inorganic systems because aqueous solutions can be employed. In addition, the vibrational energies of metal-ligand bonds are generally in the range of 100 to 700 cm^{-1}, a region in which IR is experimentally difficult to study. Such metal-ligand vibrations are frequently Raman active and readily observed by Raman spectrometry.

Inorganic materials active as catalysts or promoters are easily studied by Raman spectrometry, since supporting materials (typically SiO_2, Al_2O_3, etc.) are normally poor Raman scatterers and do not interfere with the study of the active phase. Moreover, an *in situ*, real time, noninvasive Raman mode is easily executed, thus enabling one to study catalytic materials under experimental conditions, including a broad range of temperatures and pressures and flow of gas reactants. For example, zeolites are used as catalyst in a number of processes such as petroleum cracking, NO_x reduction, isomerization, alkylation, and dealkylation reactions [58]. Jakupca and Dutta [58] used the resonance Raman technique to examine the weak acid sites of a zeolite surface, since much of the characterization has previously focused on the acid sites located inside the cages of zeolites.

Organic Applications

Raman spectrometry has been applied to organic systems, since the 1930s, because Raman spectra are useful for functional group detection and the fingerprint regions permit the identification of specific compounds. Raman scattering is particularly useful for such functional groups as $-C-S-$, $-S-S-$, $-C-C-$, $-N=N-$, and

−C=C−; infrared spectrometry is well suited to identify such functional groups as −O−H−, C=O, S=O, P=O, and $-NO_2$. Because of their complementary nature, Raman spectrometry is often used in conjunction with IR to give qualitative and structural information.

Polycyclic aromatic hydrocarbons (PAHs) are highly carcinogenic compounds that can be easily detected by resonance Raman spectrometry owing to their strong absorption of in-plane $\pi \rightarrow \pi^*$ transitions of the ring system. Asher and coworkers [59,60] have demonstrated that resonance Raman excitation of coal-derived liquid distillates selectively excites PAH species.

CHAPTER 4
DIAGNOSTICS OF INCOHERENT RESONANCE RAMAN SPECTROMETRY

Incoherent lamps were the only sources used in Raman spectrometers before the laser was introduced in 1960. At that time, the most useful radiation sources were provided by arc lamps, especially one kind of mercury arc lamp called the "Toronto lamp, " which had mercury pool electrodes cooled by water to reduce the vapor pressure of mercury. After the laser was introduced as a source for Raman spectrometry by Porto and Wood in 1962 [13], incoherent sources were replaced by lasers. New incoherent sources combined with today's dispersion and detector systems might be an inexpensive and viable alternative for the laser Raman spectrometer. In this chapter, several incoherent sources will be evaluated and will be combined with several different sample cells to obtain the best instrumental conditions.

The diagnostical experiments discussed here were all measured with a double monochromator (model 1680, Spex Industries, Edison, New Jersey) and a Hamamatsu R955 PMT which was maintained at -40^{0}C in a cooled detector housing (Products for Research Inc., Danvers, Massachusetts).

Excitation Sources

There are two requirements for incoherent sources for these studies. First, they must have a small size so that the whole instrument can be simple and compact. Second, they should have at least one strong emission line in the UV region (e.g. < 260 nm) and low intensities of other lines near this major emission line, in order to obtain a simple and reduced fluorescence background Raman spectrum.

Electrodeless Discharge Lamp

The electrodeless discharge lamp (EDL) is a very intense atomic line source which has been used in atomic fluorescence spectrometry and in atomic absorption spectrometry for elements such as As, Se, Te, and Hg. For these elements, EDLs are used instead of hollow cathode lamps, which have relatively low intensities [61].

The EDL used in this dissertation was made by Opthos Instruments, Inc. (Rockville, Maryland). It is basically a sealed quartz tube, as shown in Figure 4-1, containing a few torr of an inert gas and a small amount of metal (or salt of the metal) whose spectrum is desired. The lamp has no electrodes, hence the name, and is operated in an intense RF or microwave field, directed on the lamp by an antenna or held within a waveguide cavity. A Tesla coil is used to start the discharge by ionizing some of the inert gas atoms. The electrons produced are accelerated by the high frequency electric component of the field; the electrons acquire enough energy to ionize other atoms and maintain a plasma. The resulting heat vaporizes the metal or metal compound, which is subsequently excited by collisions to produce the spectrum. Because the gas pressure

Figure 4-1. Electrodeless discharge lamp (EDL). The EDL is placed in an intense microwave field.

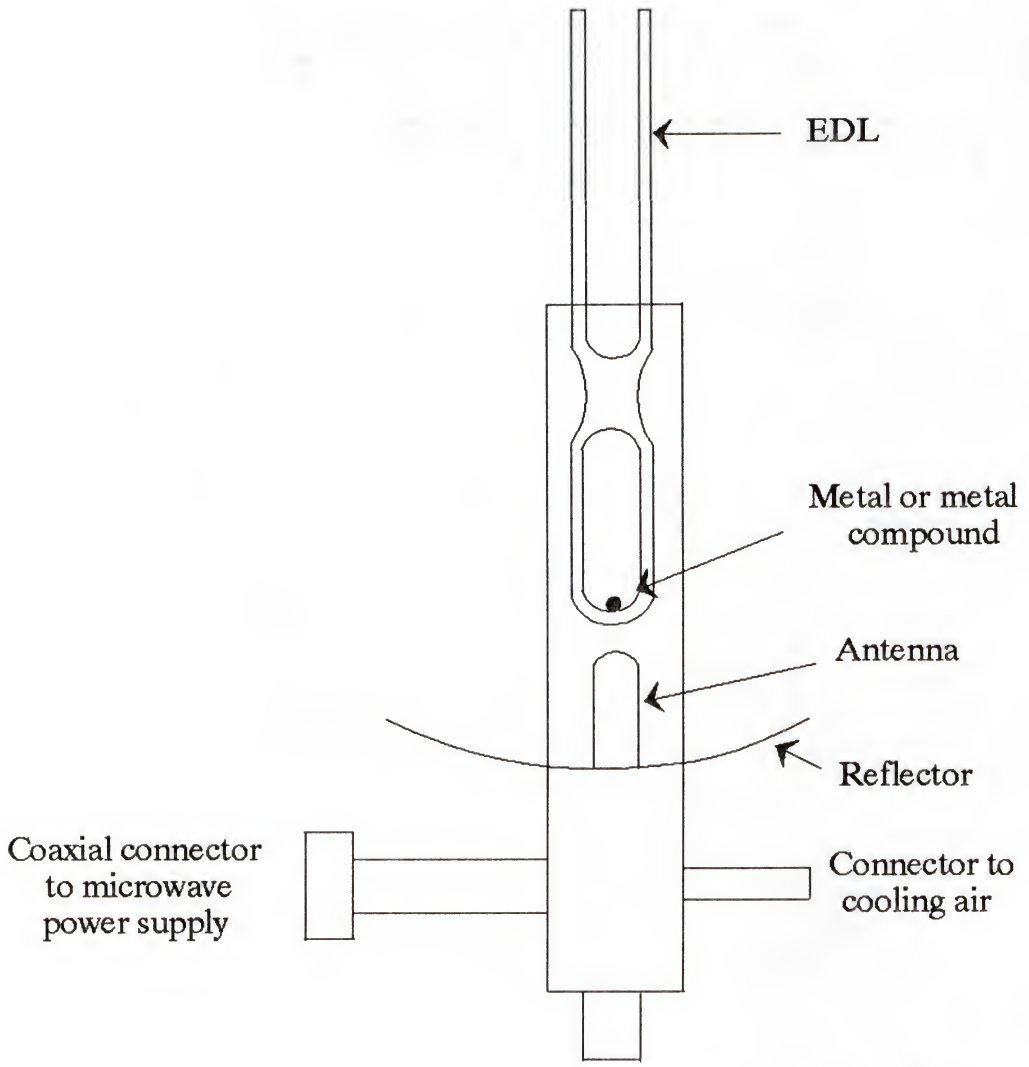
EDL
Metal or metal compound
Antenna
Reflector
Coaxial connector to microwave power supply
Connector to cooling air

and temperature are low, broadening effects are small, and narrow spectral lines result.

The Microtron model 200 (Electro-Medical Supplies, Berkshire, England) microwave generator was employed here. The Hg EDL spectrum was measured with 50 W of microwave power; the spectrum covered 250 nm to 278 nm (the spectral region for the Stokes Raman is from 0 to 3500 cm^{-1} ; see Figure 4-2). The strongest resonance line at 253.7 nm was the choice for the experiment; there were also several weak spectral lines in this region. By controlling the power supply, the Hg EDL 253.7 nm intensity increased by about 25 % as the microwave power increased from 35 W to 70 W (Figure 4-3) . However, the peak intensity is limited by a maximum power output, ~75 W, for the Microtron model 200 microwave power generator.

Low-Pressure Arc Lamps

When an arc discharge is ignited between electrodes in a low-pressure metal atmosphere (< 10 mm Hg), a diffuse discharge is produced with sharp atomic lines. There are two types of low-pressure arc lamps: a hot-cathode type which operates at relatively low voltage (~105 to 150 V ac); and a cold cathode type that starts and operates at higher voltages (start voltage: ~600 to 1500 V; operate voltage: ~145 to 600 V). In this dissertation, several small size, cold-cathode type, Pen-Ray lamps for Zn (213.9 nm), Cd (228.8 nm), and Hg (253.7 nm) were tested.

Schematic diagrams of Zn (model Z-800), Cd (model CD-480), and Hg (model 11 SC-1) Pen-Ray lamps (all from Ultra-Violet Products, Inc., San Gabriel, CA) used here are shown in Figure 4-4. From Figures 4-5 to 4-7, the spectra show that all three Pen-Ray lamps have a strong emission line in the UV region with low interference peaks near

Figure 4-2. Output of Hg EDL (50 W) over spectral range of 250 - 278 nm.

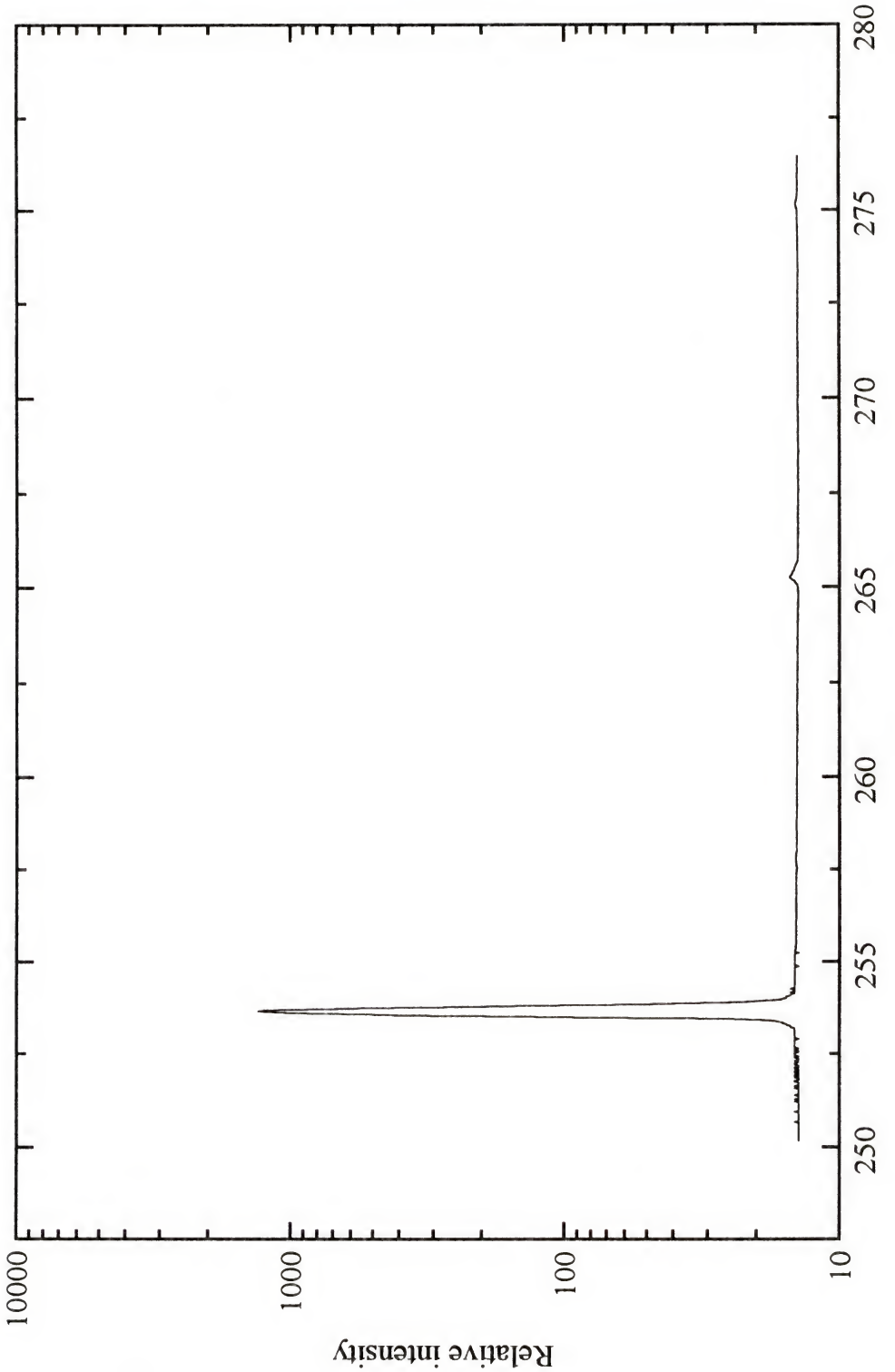
Relative intensity
10000
1000
100
10
250
255
260
265
270
275
280
Wavelength (nm)

Figure 4-3. Variation of Hg EDL 253.7 nm intensity as a function of different forward power (error bar = ± one standard deviation).

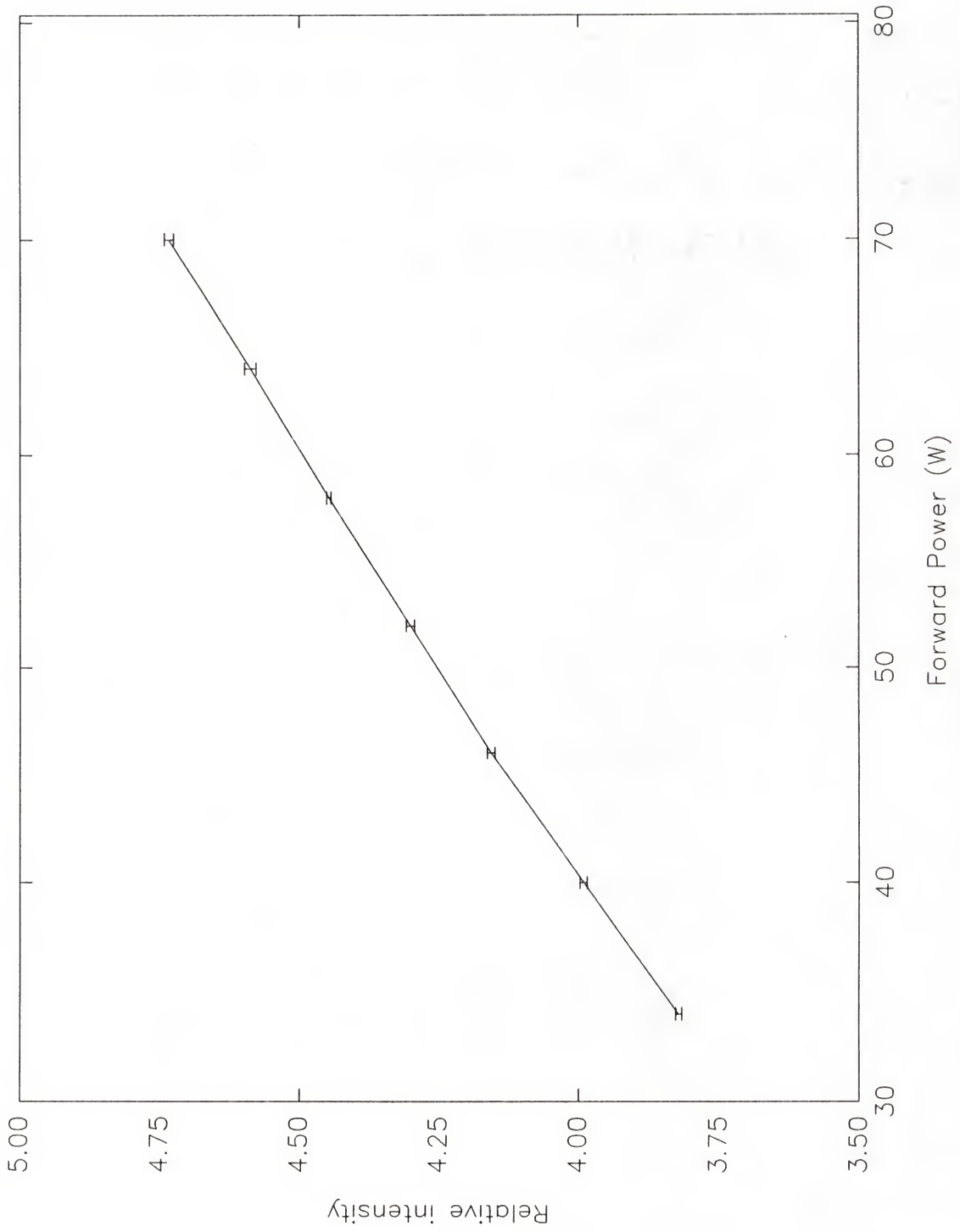
5.00
4.75
4.50
4.25
4.00
3.75
3.50
Relative intensity
30
40
50
60
70
80
Forward Power (W)

Figure 4-4. (a) Hg Pen-Ray lamp covered with a lamp shield (8 x 16 mm window).
(b) Zn Pen-Ray lamp (projected arc area 2.5 x 20 mm).
(c) Cd Pen-Ray lamp (projected arc area 2.5 x 24 mm).

(a)

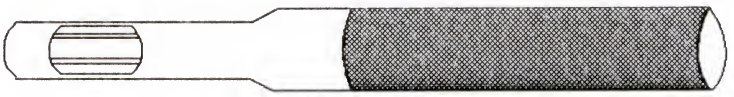

(b)

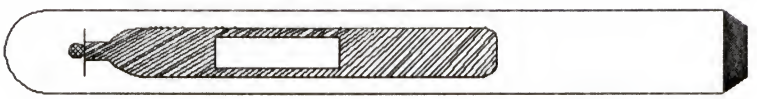

(c)

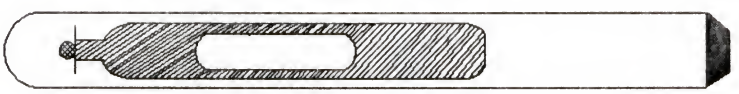

Figure 4-5. Output of Zn Pen-Ray lamp over spectral range of 220 - 231 nm.

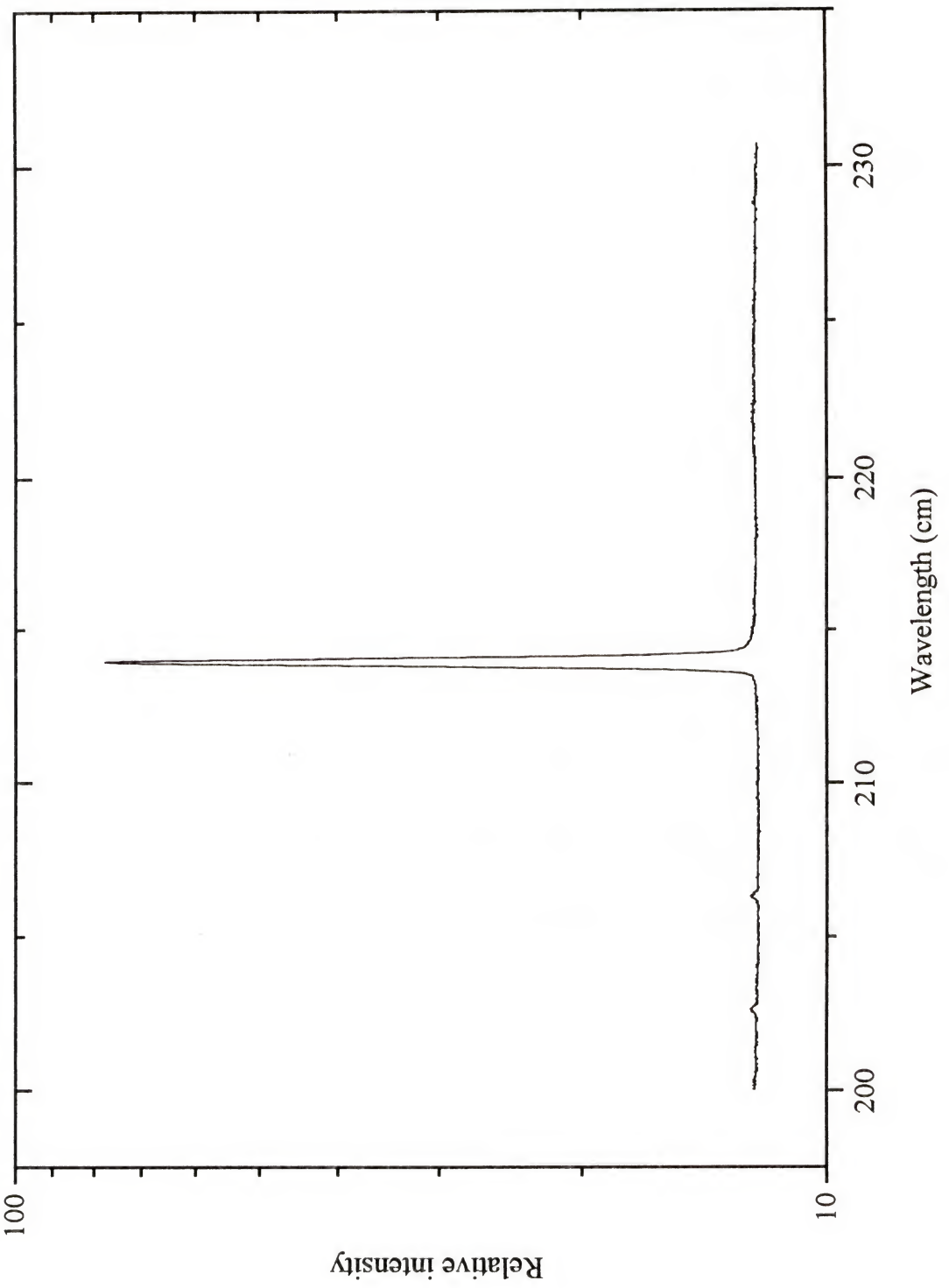
Relative intensity
100
10
200
210
220
230
Wavelength (cm)

Figure 4-6. Output of Cd Pen-Ray lamp over spectral range of 213 - 247 nm.

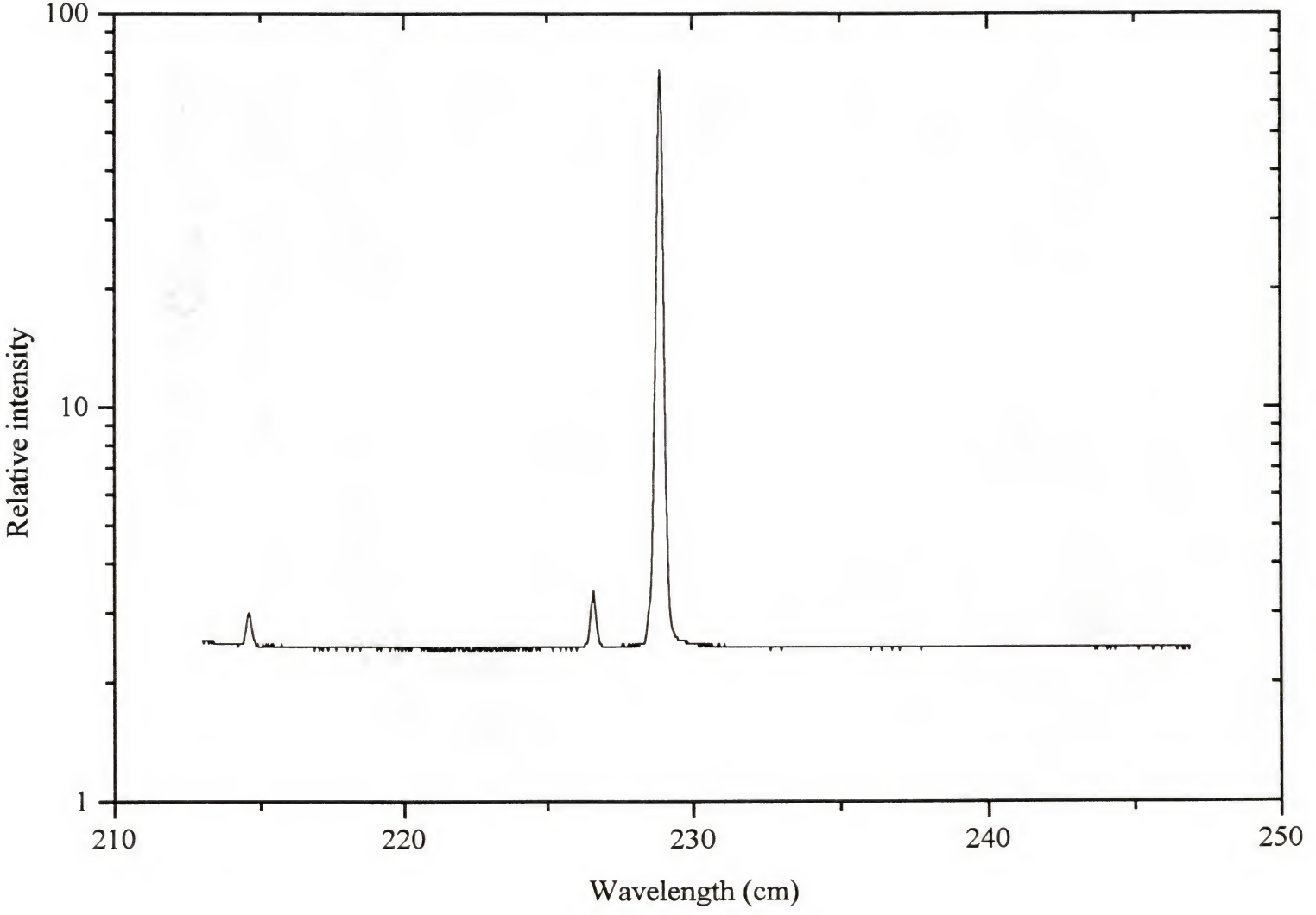
100
10
1
Relative intensity
210
220
230
240
250
Wavelength (cm)

Figure 4-7. Output of Hg Pen-Ray lamp over spectral range of 250 -278 nm.

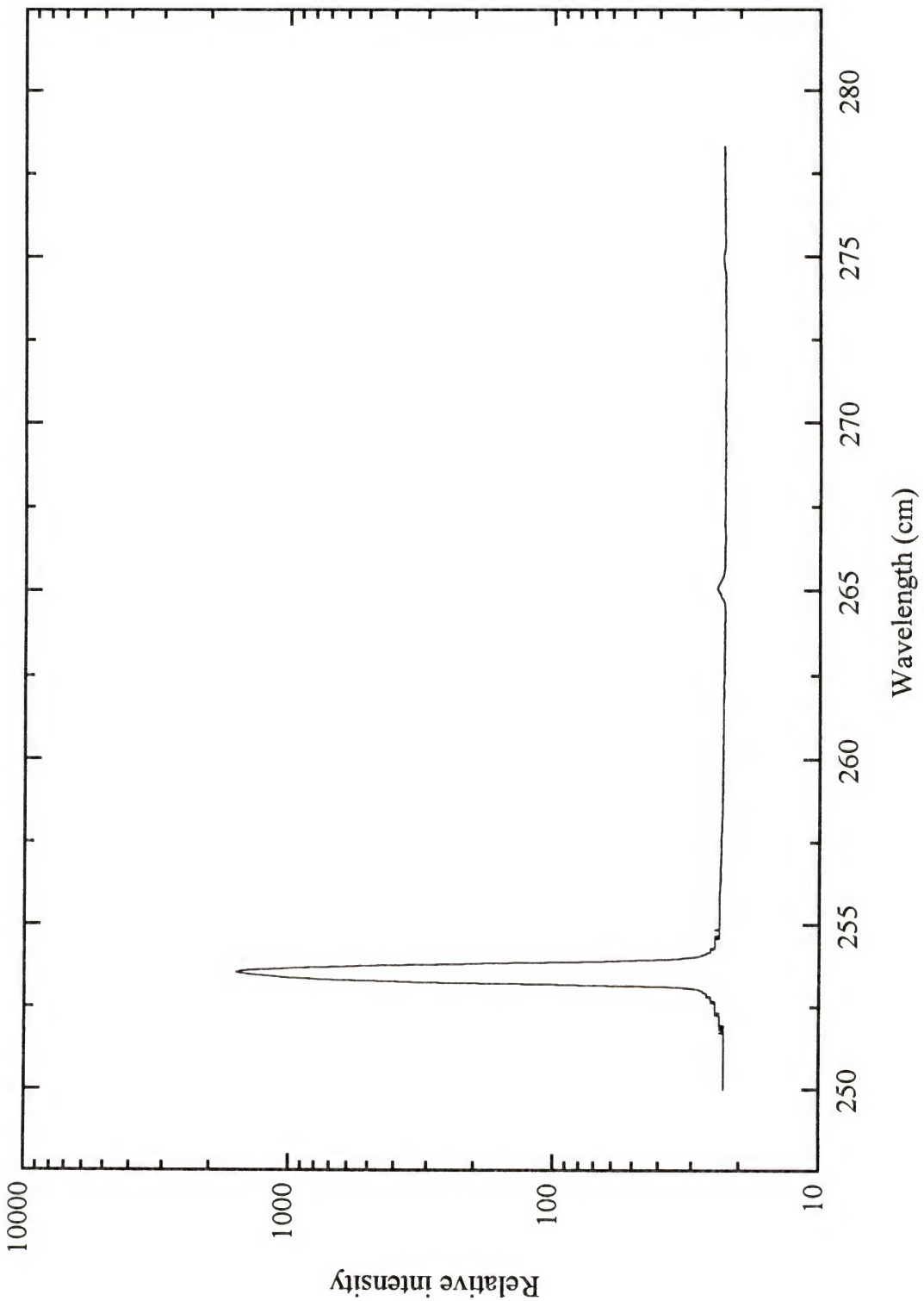
Relative intensity
10000
1000
100
10
250
255
260
265
270
275
280
Wavelength (cm)

their major emission line. The irradiance of the Hg Pen-Ray lamp was measured by using a Spectroline Model DM-254N ultraviolet meter (Figure 4-8a). From a comparison of the relative intensities of the Hg EDL and the three Pen-Ray lamps (Figure 4-8b), the Hg Pen-Ray lamp had the highest intensity and was chosen for the rest of the incoherent resonance Raman studies.

Sample Cells

The sample cells were specially designed for flowing liquid to minimize sample photodecomposition. A variety of flow cells have been used by different groups. Reider et al. [62], designed a thin, stable membrane flow cell, formed by a nozzle and two wires, which could reach a maximum separation of $\sim$15 mm wide and $\sim$50 μm thick. Asher and coworkers [63] used a jet nozzle to get an optically uniform stream about 3 mm high, 0.2 mm wide, and 200 μm thick. Lin et al. [47] made a cylindrical windowless cell with height and diameter of about 2 mm. In this section, three different flow cells, a membrane flow cell, an index matched cell, and a fluorescence flow cell were evaluated.

Membrane Flow Cell

The membrane flow cell was a similar design to the one used by Reider et al. [62]. Figure 4-9 shows the principle of the design. The sample solution is pumped by a syringe pump to the end of a needle, which is extended by two thin stainless steel tubes. The membrane formed between these two wires is increased gradually to reach

Figure 4-8. (a) Hg Pen-Ray lamp was measured using a Spectroline Model DM-254N ultraviolet meter. (b) Relative intensities of Pen-Ray lamps, Zn (213.9 nm), Cd (228.8 nm), and Hg (253.7 nm), and EDL Hg (253.7 nm).

(a)

Distance from meter	Power per unit area
No distance	4.2 (mW/cm^2)
0.5 cm	3.2 (mW/cm^2)
1cm	1.3 (mW/cm^2)

(b)

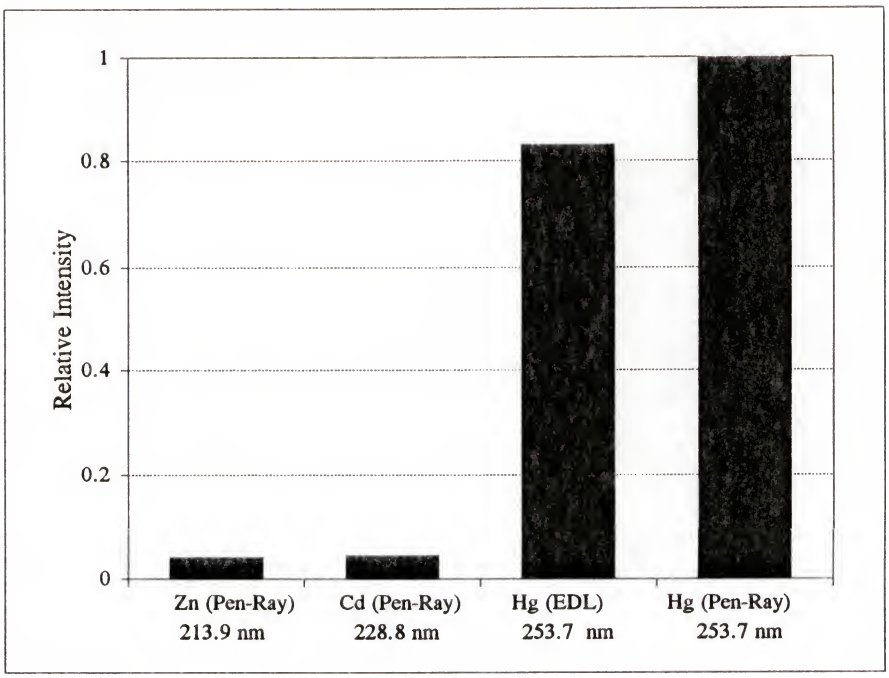

Figure 4-9. Membrane flow cell for resonance Raman spectrometry.

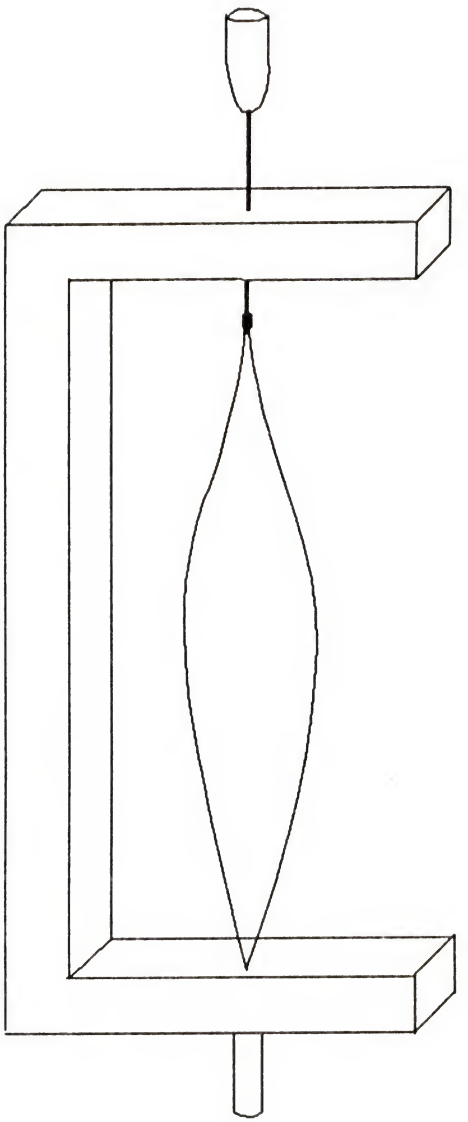

a maximum width of about 10 mm and then is gradually reduced again. A ⊏-shaped aluminum holder is used to hold the membrane cell. This flow cell was not chosen for the final experimental setup because the membrane was difficult to form with some low viscosity solvents (e.g. acetonitrile). By adding a surfactant, the viscosity may increase but it also changes the solvent polarity, causing dissolution problems.

Index Matched Cell

The index matched cell shown in Figure 4-10 was designed to connect to a capillary column so that it could be used as an on line detector for a separation system. A stainless steel cell with a 1" diameter quartz window on both sides was used as a container for the index matching fluid. The experiment was designed by passing a 200 μm ID capillary column through the cell with the Pen-Ray lamp placed next to it (inside the cell) and the Raman signal collected at 90^0 through one of the quartz windows. An appropriate index matching fluid is one with a low absorption of excitation source flux, weak Raman scattering, and a refractive index close to the refractive index of the capillary column wall to reduce scattered light from the column. This index matched cell was evaluated and discarded because only a small portion of incident radiation from the Pen-Ray lamp illuminated the sample, causing the Raman scattering to be too weak to measure.

Fluorescence Flow Cell

A commercial 1-cm cuvette fluorescence flow cell is shown in Figure 4-11. It is made of quartz with three transparent sides and one opaque side. Sample flows through an inlet (near the opaque side) into a small compartment then goes into a large

Figure 4-10. Index matched cell for resonance Raman spectrometry.

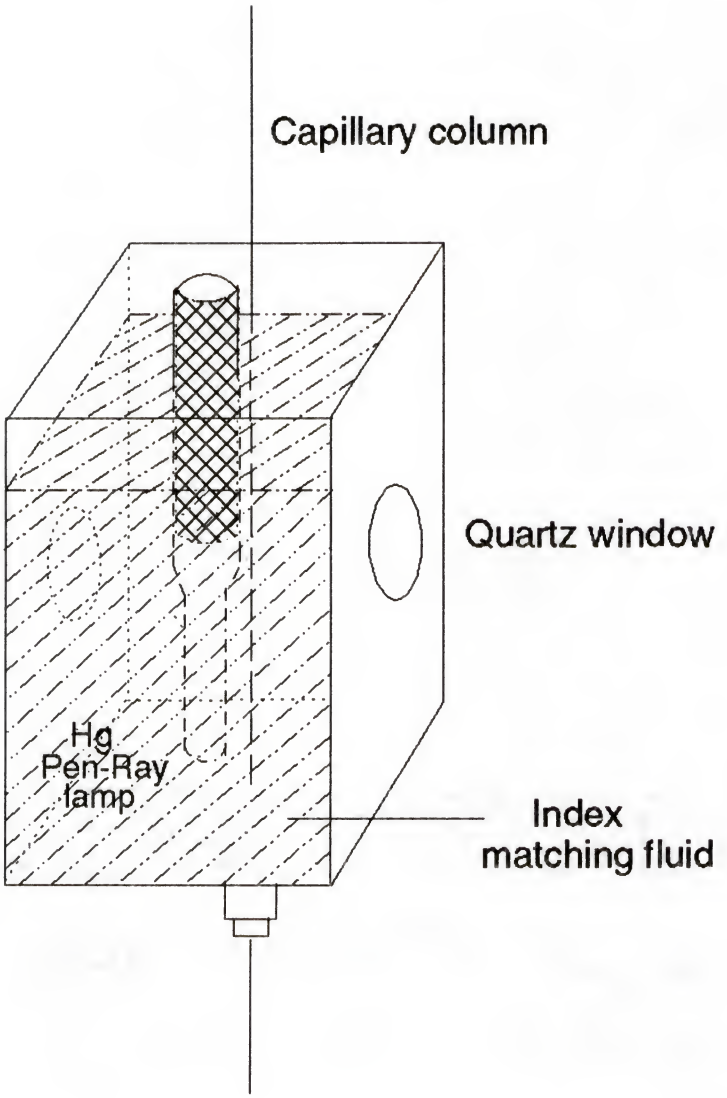
Capillary column
Quartz window
Hg
Pen-Ray
lamp
Index
matching fluid

Figure 4-11. A 1-cm fluorescence flow cell for resonance Raman spectrometry.

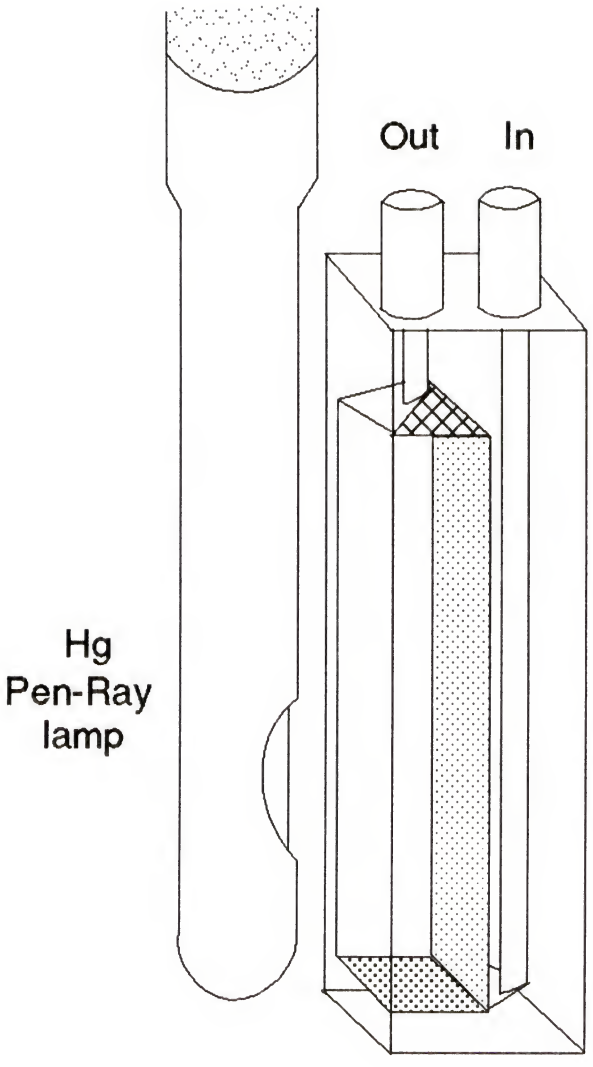
Out
In
Hg
Pen-Ray
lamp

compartment at the bottom; the sample solution flows to the top and then reaches the outlet. The Pen-Ray lamp was placed adjacent to the transparent wall of the cell next to the outlet (see Figure 4-11). Because the Pen-Ray lamp ($\sim$6 mm diameter) is covered with a shield containing a hole (8 x 16 mm), it can totally illuminate the sample in the 1-cm flow cell. The fluorescence flow cell resulted in the largest Raman signals, and so was selected as the sample cell for the incoherent resonance Raman spectrometer system used in the studies in this dissertation.

Experimental Setup

A schematic diagram of the experimental apparatus is shown in a block diagram in Figure 4-12. The source and sample flow cell have been discussed earlier. The flow cell was pumped by an Altex model 110A HPLC pump.

Spectrometer/spectrograph. A model 1680 double-grating 0.22 m focal length monochromator (Spex industries, Edison, New Jersey) was used with a grating (1200 grooves/mm) blazed for 250 nm. The reciprocal linear dispersion was 1.8 nm/mm, or about 290 cm^{-1}/mm in the spectral region under study. Collection optics were oriented at 90^0 to the emission axis, and the image collection was matched to the monochromator's effective f number of 3.9. By using a 1:1 image and 100 μm monochromator slit with 1-cm cuvette flow cell, the detection volume was about 10 μl.

Detector/amplifiers. A Hamamatsu R955 photomultiplier maintained at -40^0 C in a thermoelectric cooled housing (Products for Research Inc., Danvers, Massachusetts)

Figure 4-12. Experimental setup. The Pen-Ray lamp is set directly adjacent to the 1-cm cuvette flow cell. A flat black cardboard baffle is placed next to the lamp to prevent the access of the Pen-Ray light to the monochromator.

Top view

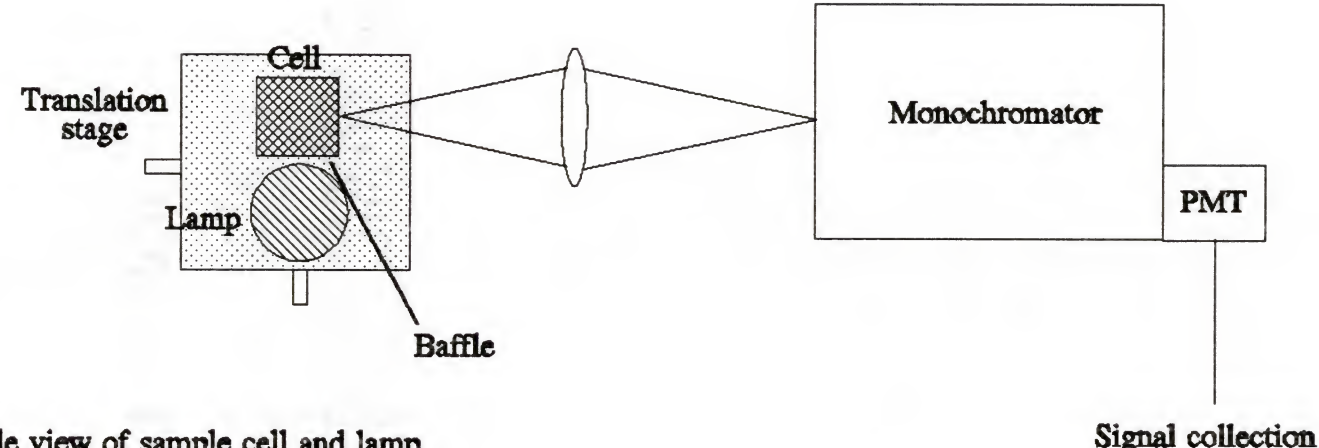

Side view of sample cell and lamp

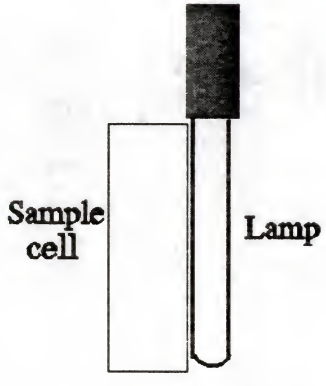

was used as the detection assembly. The output current was converted to voltage by a Thorn EMI A1 I/V converter, and then amplified by a Textronix 26A2 differential amplifier (or converted to voltage and amplified by Keithley 427 current amplifier, Keithley Instruments Inc., Cleveland, Ohio). Analog low-pass filtering was obtained with a SR235 analog processor (Stanford Research Systems. Sunnyvale, CA).

Interface/computer. The signal was collected through a Stanford Research Systems SR245 computer interface to a IBM-compatible 386 personal computer.

System Optimization

Flow Rate Optimization

In this experiment, anthracene (99.9%, Aldrich) was chosen as the model analyte because it has good Raman scattering (Figure 4-13) and a maximum absorption close to the Hg excitation line at 253.7 nm (Figure 4-14). The UV transparency and anthracene solubility characteristics made acetonitrile (HPLC grade Fisher Scientific) a very good solvent for this work.

By using the 10^{-4} M anthracene solution with, the 1-cm cuvette flow cell and controlling the flow rate with a HPLC pump, the variation of the Raman signal with sample flow rate for anthracene is shown in Figure 4-15. The signal increased with increasing sample flow rate until 3.5 ml/min, where the signal became constant for all higher flow rates. The decreased signal at lower flow rates was a result of photodecomposition.

Figure 4-13. Raman Spectrum of 10^{-4} M anthracene solution in acetonitrile.

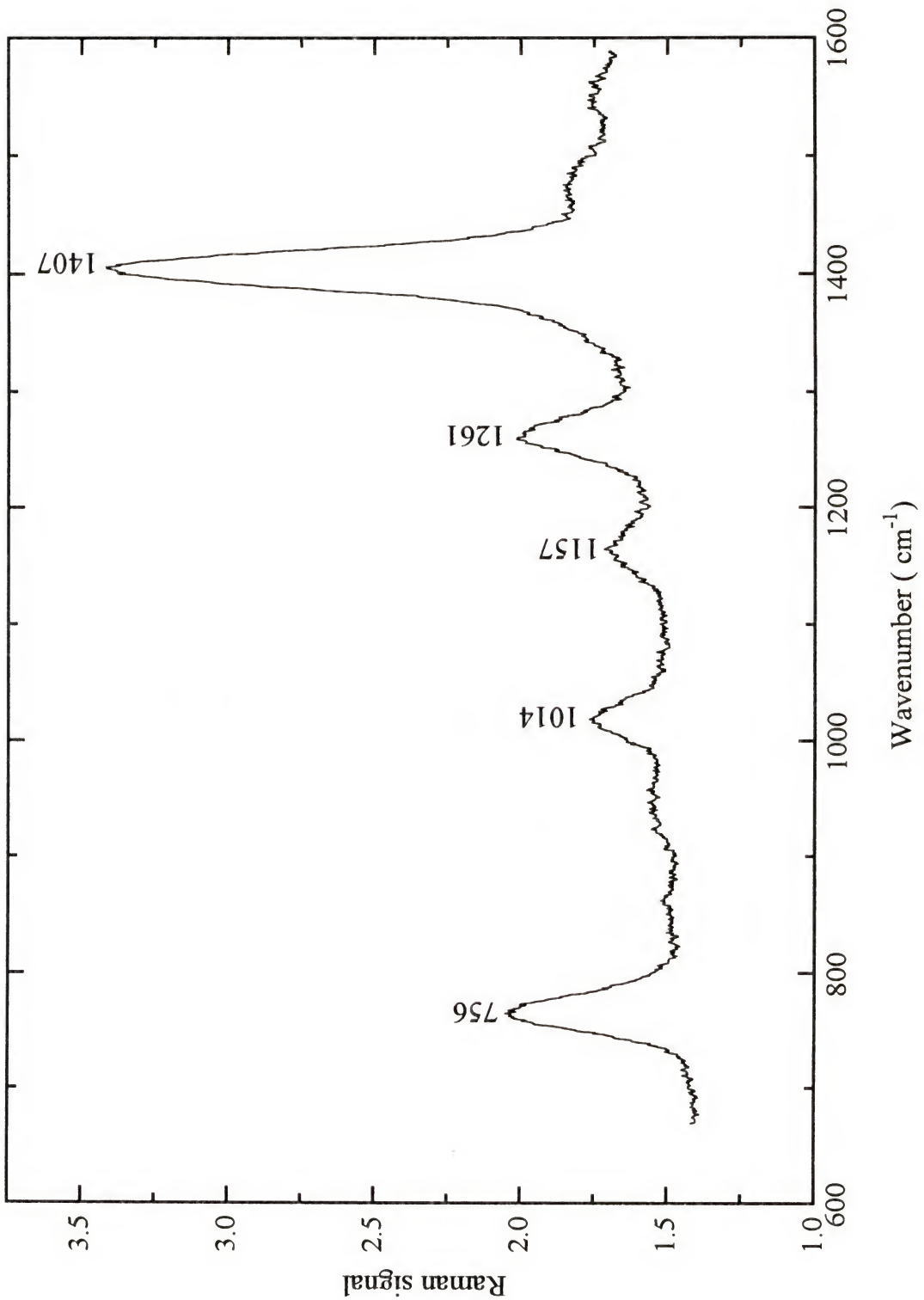
Raman signal
3.5
3.0
2.5
2.0
1.5
1.0
600
800
1000
1200
1400
1600
Wavenumber (cm-1)
1407
1261
1157
1014
756

Figure 4-14. Absorbance spectrum of 10^{-5} M of anthracene solution in acetonitrile.

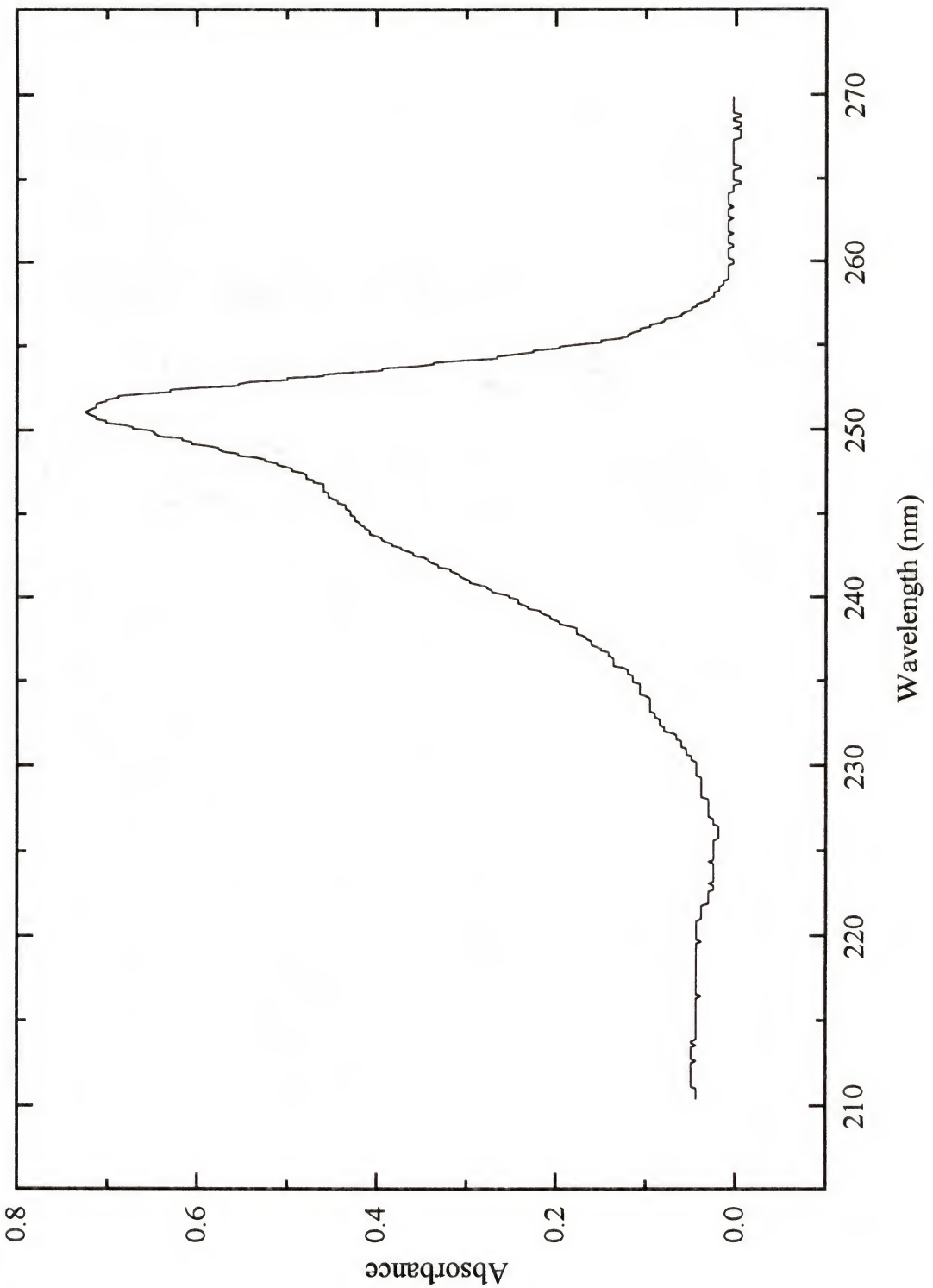
0.8
0.6
0.4
0.2
0.0
Absorbance
210
220
230
240
250
260
270
Wavelength (nm)

Figure 4-15. Variation of intensity of anthracene Raman peak, 1407 cm^{-1}, as a function of sample flow rates. Anthracene concentration was 10^{-4} M.

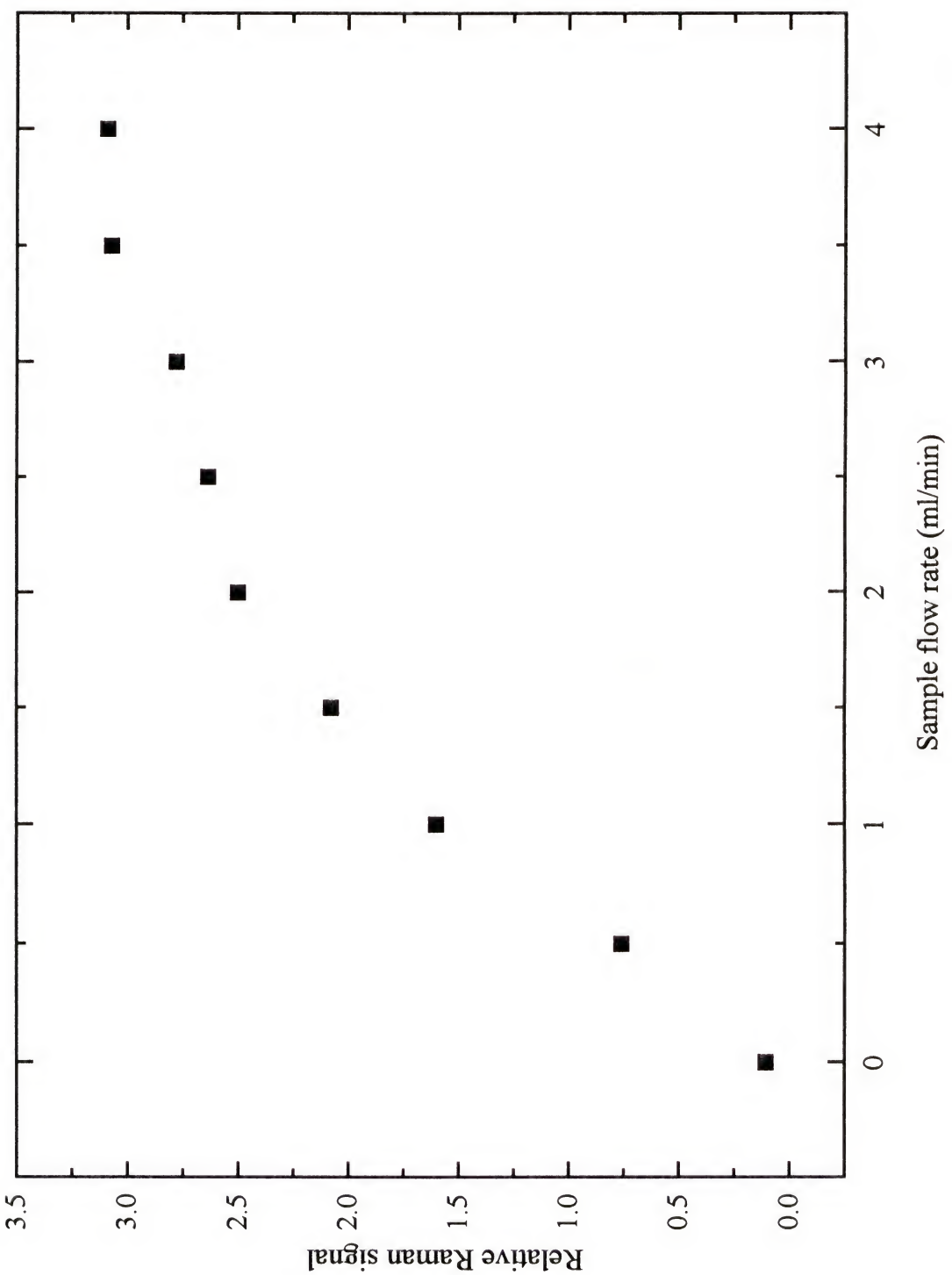
Relative Raman signal
0.0
0.5
1.0
1.5
2.0
2.5
3.0
3.5
0
1
2
3
4
Sample flow rate (ml/min)

PMT High Voltage Optimization

A model R955 photomultiplier made by Hamamatsu was used as the detector; the detector has a high sensitivity multialkali (Na-K-Sb-Cs) photocathode with a synthetic silica window. The best anode to cathode supply voltage was obtained by maximizing the signal-to-noise ratio. The experimental conditions used here were the same as in the flow rate optimization experiment except for the fixed sample flow rate was at 4.0 ml/min. The most intense peak, 1407 cm^{-1}, for anthracene was selected to optimixe the signal-to-noise ratio. Figure 4-16 shows the best anode to cathode voltage is 1000 V.

Sample Absorption Correction

It has long been recognized [64] that sample absorption has a pronounced effect on relative intensity measurements in resonance Raman spectroscopy. Observed Raman scattering intensities in different regions of the sample cell may be affected differently by sample absorption (see Figure 4-17) and individual Raman bands will be differently attenuated because the sample absorbance varies with wavelength. Moreover, Raman scattering is proportional to the sample concentration and intensity of incident radiation; however, the sample concentration attenuates both the incident and the Raman scattering radiation in an exponential manner. As a result, a plot of observed Raman scattering intensities vs. analyte concentration may be far from linear and may reach a maximum.

The degree to which sample absorption affects a resonance Raman measurement depends on the magnitude and band shape of the sample absorption spectrum and the

Figure 4-16. Variation of signal-to-noise ratio of the anthracene Raman peak, 1407 cm^{-1}, as a function of high voltage applied to Hamamatsu R955 PMT. Anthracene concentration was 10^{-4} M.

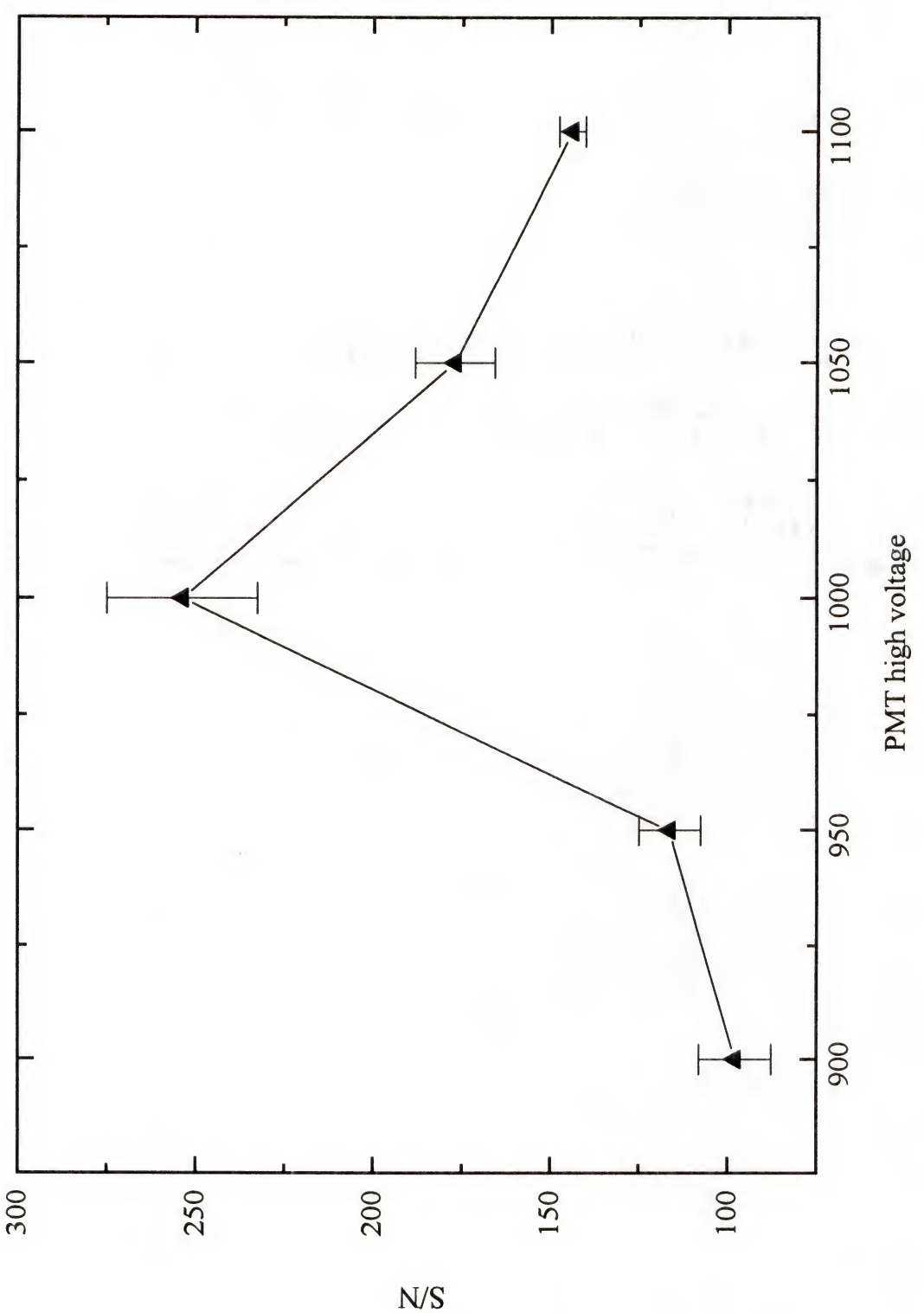
S/N
300
250
200
150
100
900
950
1000
1050
1100
PMT high voltage

Figure 4-17. Raman signal of the anthracene 1407 cm^{-1} peak as a function of translation stage position in the Pen-Ray light emission axis for 10^{-3} M to 10^{-6} M anthracene solutions.

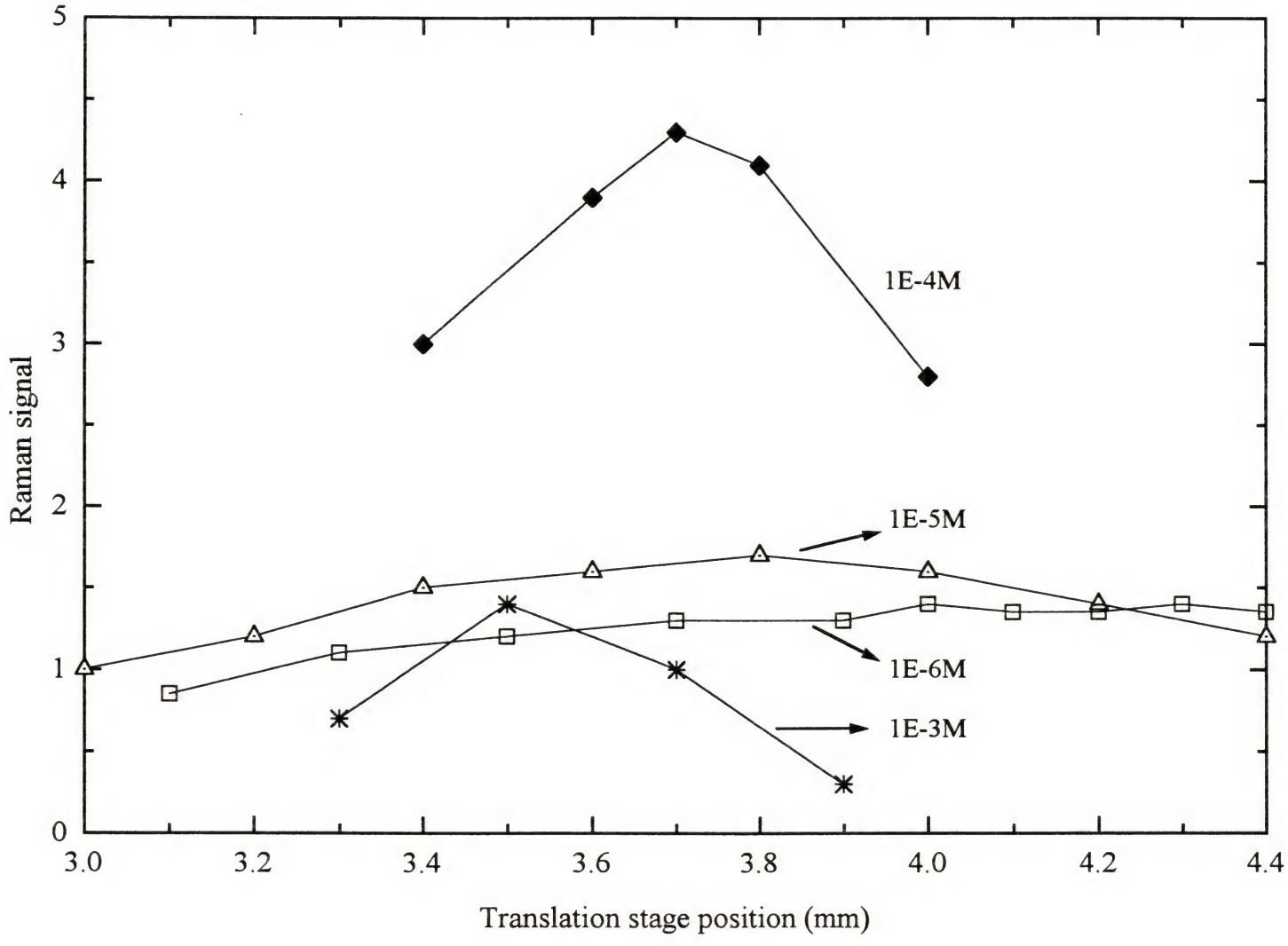
Raman signal
Translation stage position (mm)
1E-4M
1E-5M
1E-6M
1E-3M
0
1
2
3
4
5
3.0
3.2
3.4
3.6
3.8
4.0
4.2
4.4

geometry of the scattering experiment. Earlier sample absorption effects on Raman scattering intensity were studied in several papers [65,66]. In this dissertation, a model has been designed to examine the sample absorption effect with a 1-cm flow cell. The anthracene Raman peaks, 756 cm^{-1} and 1407 cm^{-1} (see Figure 4-13), were selected for intensity comparison. In Figure 4-18, the absorption spectrum of anthracene is given; the Raman peaks at 756 cm^{-1} and 1407 cm^{-1} occur at wavelengths where anthracene has a molar absorptivity, ϵ, of 7.21 and 2.35 mM^{-1} cm^{-1}, respectively. The pathlengths involved with excitation and Raman scattering are shown schematically in Figure 4-19. The observed Raman radiant power, Φ_{obs}, in W, is a consequence of the exponential reduction in power (Beer's law) on passage of the scattered light through the sample

$$\Phi_{obs} = \Phi_s \, 10^{-yc\epsilon} \tag{4.1}$$

where Φ_s, in W, is the intrinsic Raman radiant power at point "s", c is the molar concentration of absorbing molecules, in mol L^{-1}, y is the scattering path length from s point to the cell wall, in cm, and ϵ, is the molar absorptivity at the scattering wavelength, in L mol^{-1} cm^{-1}. The radiant power ratio, R, for two different Raman scattering peaks, 756 cm^{-1} and 1407 cm^{-1}, is given by

$$R_{obs} = R_s \, 10^{-yc\Delta\epsilon} \tag{4.2}$$

where $\Delta\epsilon$ is the difference in absorptivity at two scattering wavelengths.

$$\log R_{obs} = \log R_s - yc\Delta\epsilon \tag{4.3}$$

A plot of equation 4-3 is shown in Figure 4-20. A straight line with a slope of 0.313 cm implies y is effectively constant under the experimental conditions. For the 1-cm flow cell, with the Pen-Ray lamp placed adjacent to the middle of the cell wall, the expected

Figure 4-18. Absorption spectrum of anthracene showing positions of the exciting line (253.7 nm) and two Raman bands, 756 and 1407 cm^{-1}.

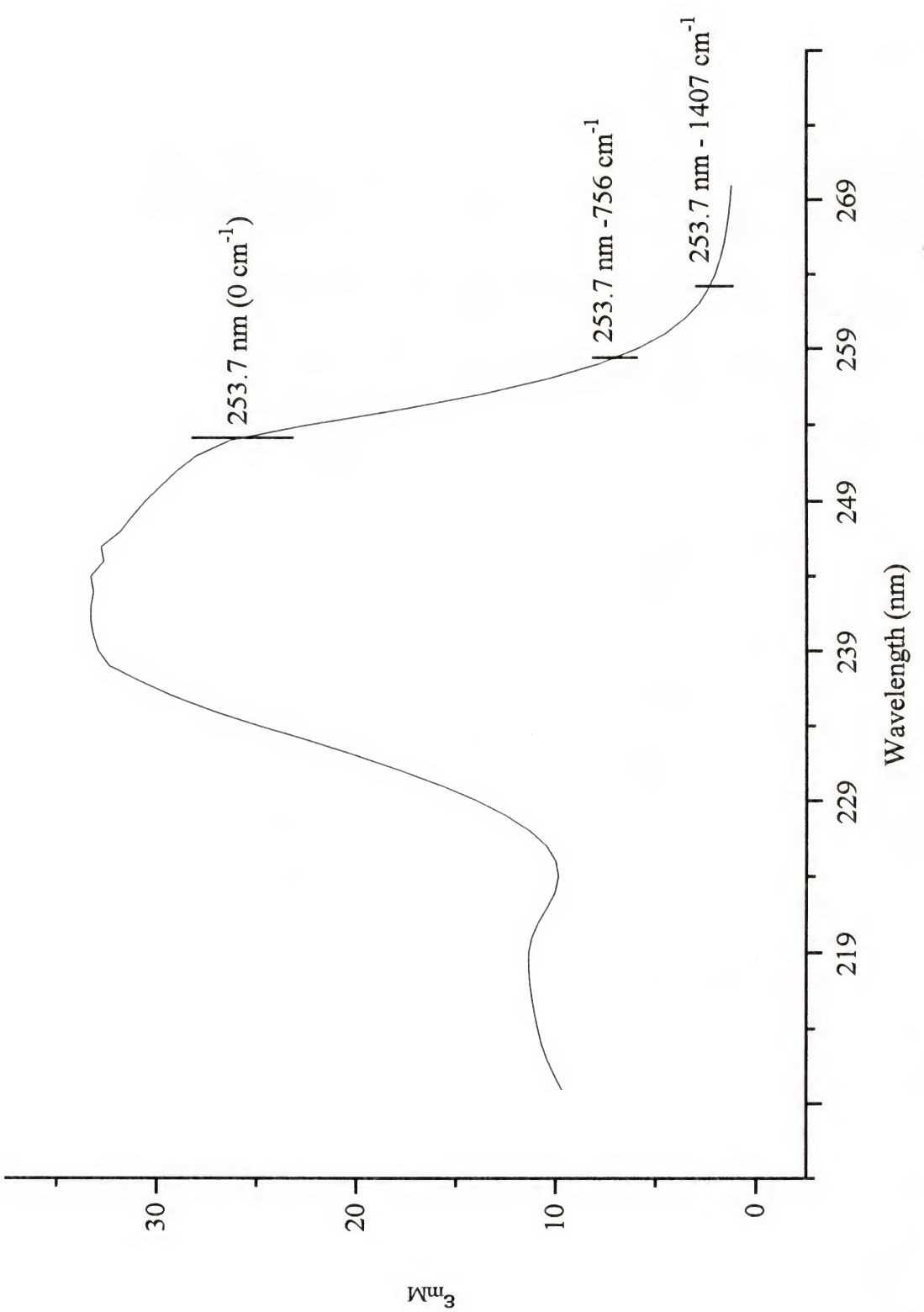
253.7 nm (0 cm-1)
253.7 nm -756 cm-1
253.7 nm - 1407 cm-1
Wavelength (nm)
219
229
239
249
259
269
0
10
20
30
εmM

Figure 4-19. Schematic diagram showing excitation and scatter directions.

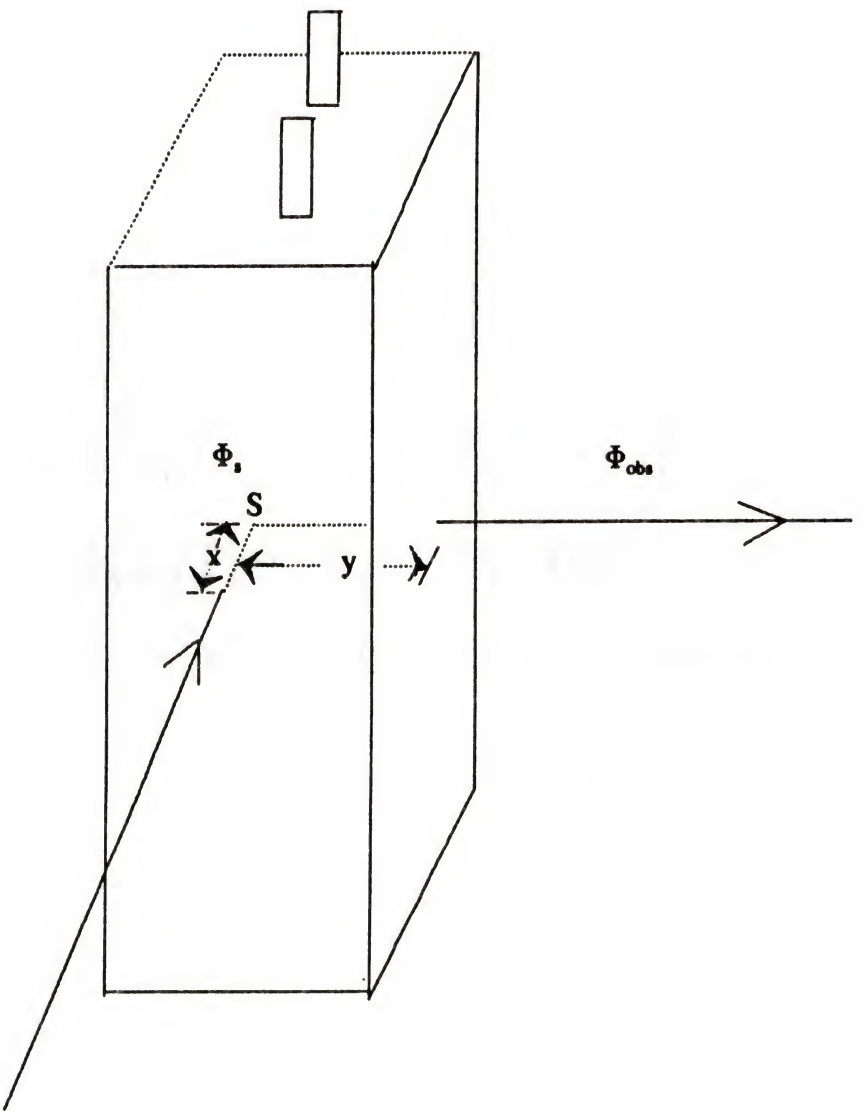
Φs
Φobs
S
x
y

Figure 4-20. Experimental plot for the logarithm of the observed power ratio of the anthracene Raman bands at 756 and 1407 cm^{-1} versus the product of concentration and the absorptivity difference at the two scattering frequency. The line is linear with a slope of 0.313 cm which is the effective scattering path length.

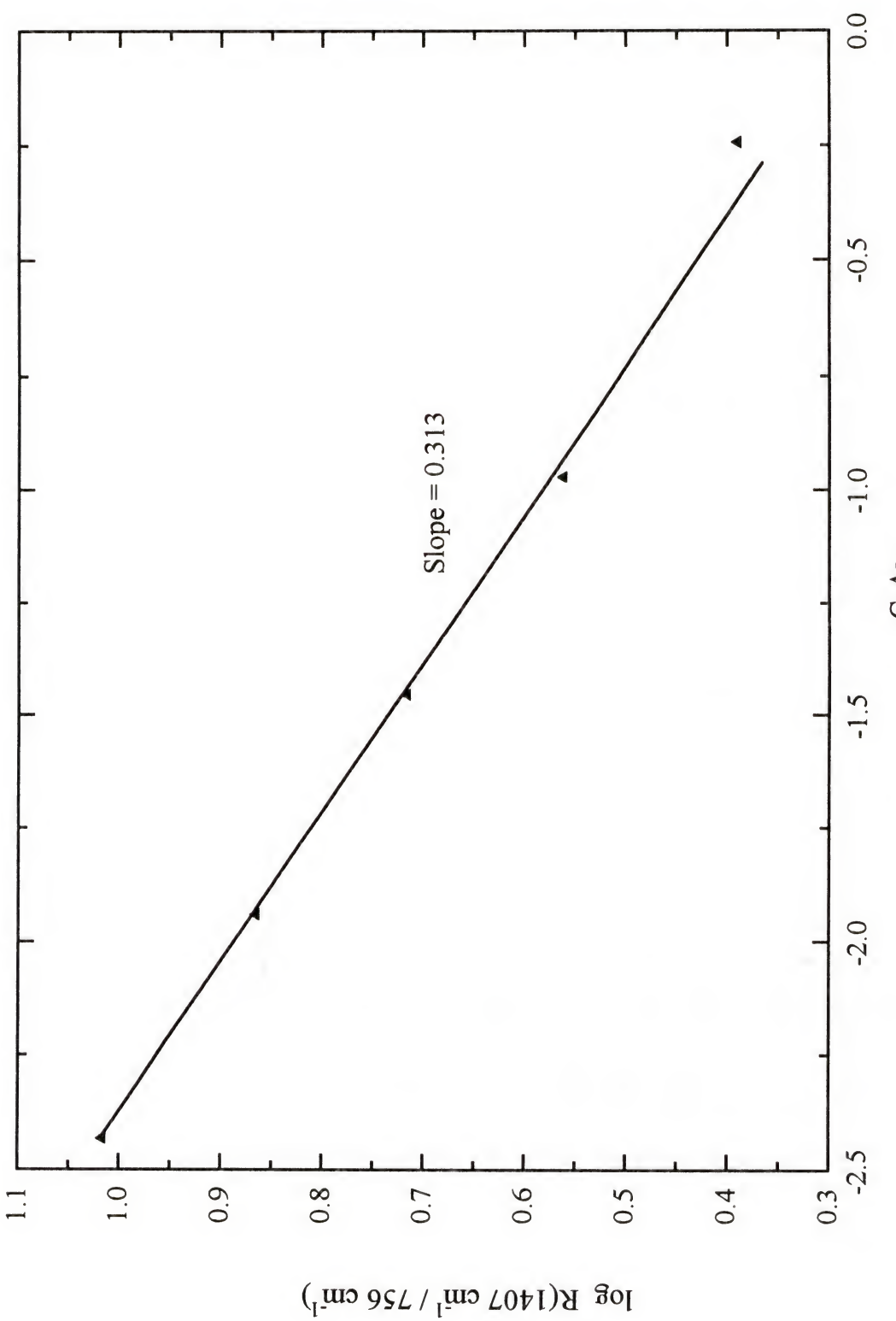
Slope = 0.313
log R(1407 cm⁻¹ / 756 cm⁻¹)
C Δε
1.1
1.0
0.9
0.8
0.7
0.6
0.5
0.4
0.3
-2.5
-2.0
-1.5
-1.0
-0.5
0.0

scattering path length is 0.5 cm if scattering occurs at a point at the center of the cell. Since the actual scattering volume by the excitation Pen-Ray lamp is larger and a more complex shape, the agreement is satisfactory.

The effect of absorption on the incident radiation was also examined by measuring absorption spectra of anthracene at concentrations of 10^{-3} M, 10^{-4} M, 10^{-5} M, and 10^{-6} M and the absorption spectrum of pure acetonitrile solvent (Figure 4-21). The maximum Raman scattering was obtained at an anthracene contraction at 10^{-4} M. The 10^{-6} M anthracene and pure acetonitrile gave nearly identical spectra with predominate peaks at 918 cm^{-1} and 1376 cm^{-1} peaks from acetonitrile. The spectrum for the 10^{-4} M anthracene solution shows four peaks at about 756 cm^{-1} , 1014 cm^{-1}, 1157 cm^{-1}, and 1407 cm^{-1} from anthracene. The resolution for these experiments is $\sim$30 cm^{-1} (monochromator slit 100 μm); therefore, the 1376 cm^{-1} peak from the solvent (acetonitrile) overlaps with the 1407 cm^{-1} peak from anthracene for the 10^{-5} M anthracene solution.

The reason that the Raman scattering for the 10^{-3} M anthracene solution is weaker than the 10^{-4} M anthracene solution is that strong absorption of the incident radiation by anthracene occurs. It can be explained by a more extensive model shown in Figure 4-19. From Beer's law, The radiant power, Φ_{es}, at s point can be expressed as

$$\Phi_{es} = \Phi_0 \, 10^{-x\epsilon' c} \qquad (4.4)$$

where Φ_0 is the excitation radiant power at 253.7 nm, in W, ϵ', is the molar absorptivity, in M^{-1} cm^{-1}, at 253.7 nm, c is the anthracene concentration in M (Mol L^{-1}), x is pathlength from cell wall (close to excitation lamp) to s point, in cm. The Raman signal

Figgure 4-21. Raman spectra of pure acetonitrile and 10^{-3} M to 10^{-6} M anthracene solutions.

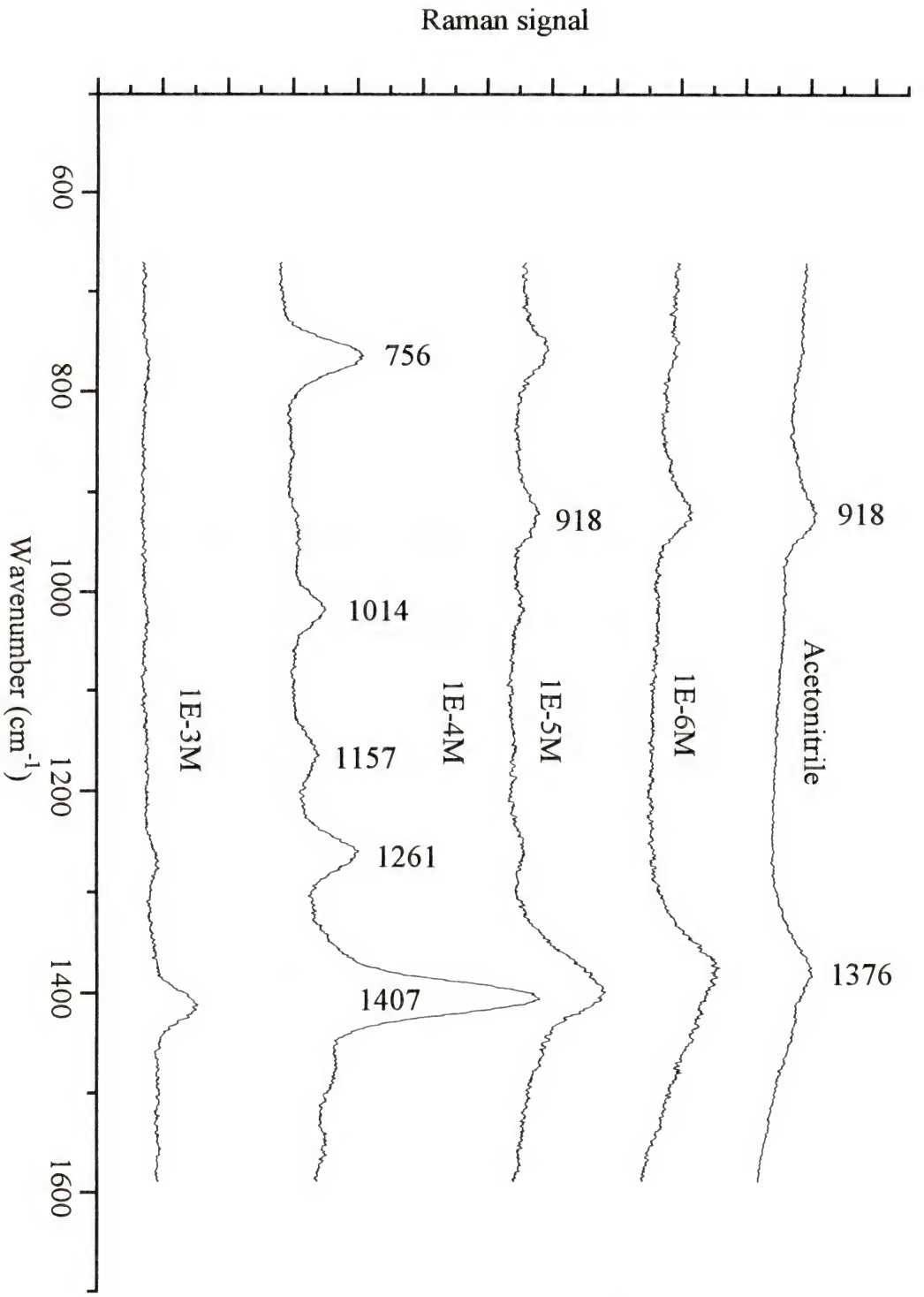
Raman signal
600
800
1000
1200
1400
1600
Wavenumber (cm-1)
1E-3M
1E-4M
1E-5M
1E-6M
Acetonitrile
756
1014
1157
1261
1407
918
918
1376

at s point, Φ_s, can be expressed as

$$\Phi_s = K\ c\ \Phi_{es} \tag{4.5}$$

where K is constant (for same experimental setup), in M^{-1}. Substitution of equation 4.4, 4.5 into 4.1 yields

$$\Phi_{obs} = K\ c\ \Phi_0\ 10^{-(y\epsilon c + x\epsilon' c)}. \tag{4.6}$$

Because the sample illuminated area is not a point, the observed Raman signal should be integrated in both the x and y directions. Equation 4.6 shows the integral equation to be used

$$\Phi_{obs} = \int_{m}^{n}\int_{o}^{p} Kc\Phi_0 10^{-(y\epsilon c + x\epsilon' c)} dy\,dx \tag{4.7}$$

where m, n, o, p, in cm, are the lower and upper limits in the x and y directions. Considering the experimental results shown in Figure 4-21, the anthracene Raman peak at 756 cm^{-1} can be used to examine the theoretical calculation given in equation 4.7 (the most intense anthracene Raman peak at 1407 cm^{-1} may overlap with peak 1376 cm^{-1}, from acetonitrile, at low anthracene concentration) . Assuming K=0.01 (anthracene is a good Raman scattering compound so that its Raman signal could be about 10^{-7} times of excitation source; however, the resonance enhancement of anthracene signal could be about 10^5 times of normal Raman signal; so K=0.01), Φ_0=4.2 mW (calculated from Figure 4-8a; the Hg Pen-Ray lamp radiant power per unit area is 4.2 mW cm^{-2} and anthracene sample illuminated area in 1-cm fluorescence flow cell is about 1 cm^2). The point m is the sample cell position in x direction where sample Raman signal was collected from point m to n in x direction through monochromator. It was uncertain and

could be estimated from Figure 4-17. Here, m equals to 0.05, 0.07. 0.09 cm were calculated in this model; n-m=0.01 cm is the width of detected sample area in x direction with monochromator slit of 0.01 cm and 1 to 1 image. Because the Hg Pen-Ray was placed in the middle of the sample cell wall and lamp outer diameter is about 0.6 cm, o and p are equal to 0.2 cm and 0.8 cm, respectively. The molar absorptivity of ϵ = 7210 M^{-1} cm^{-1} (at anthracene Raman peak, 756 cm^{-1}), and ϵ'=25000 M^{-1} cm^{-1} (at the Hg excitation wavelength, 253.7 nm) were calculated from Figure 4-18. By calculating this equation with a computer software (Mathcad 4.0), the plot of anthracene concentration vs. relative Raman signal (756 cm^{-1}) is shown in Figure 4-22.

The three m (0.05, 0.07, 0.09 cm) positions calculated from equation 4.7 all have a similar trend that shows the most intense 756 cm^{-1} Raman peak is from 10^{-4} M anthracene solution and that matches very well with the experimental result from Figure 4-21. Moreover, the experimental ratio of the anthracene Raman peak, 756 cm^{-1}, at 10^{-5} to 10^{-4} M solution is about 0.32 which is close to the theoretical calculation, 0.33, when m is equal to 0.09 cm.

Figure 4-22. Raman signal of anthracene peak, 756 cm^{-1} is theoretically calculated over a concentration from 10^{-2} M to 10^{-6} M. The point m is the sample cell position in x direction where sample Raman signal was collected; m=0.05, 0.07, 0.09 cm were calculated.

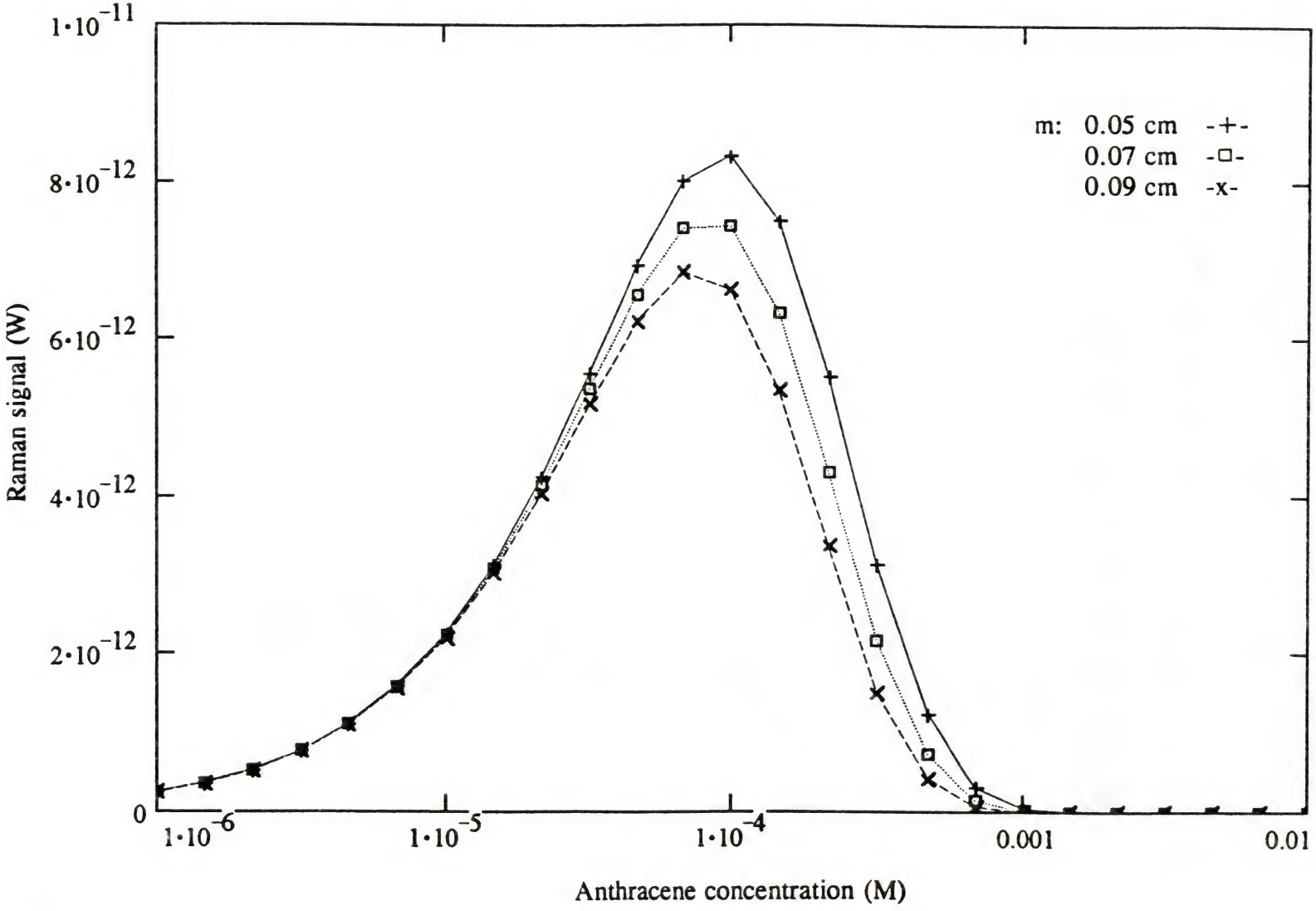
m: 0.05 cm -+-
0.07 cm -□-
0.09 cm -x-
Raman signal (W)
1·10^-11
8·10^-12
6·10^-12
4·10^-12
2·10^-12
0
1·10^-6
1·10^-5
1·10^-4
0.001
0.01
Anthracene concentration (M)

CHAPTER 5
APPLICATIONS OF INCOHERENT RESONANCE RAMAN SPECTROMETRY

Anthracene and Anthracene Derivatives

Anthracene is a very good Raman scattering compound that has been studied in several papers [67-69]. In this dissertation, it was widely used for diagnostical tests for incoherent resonance Raman spectrometry. Since anthracene molecules have D_{2h} symmetry, the rule of mutual exclusion must be satisfied. Mutual exclusion states that transitions which are permitted in Raman spectrometry are forbidden in IR spectrometry.

The molecule of anthracene contains 24 atoms, and its vibrational spectrum has 66 fundamental vibrations. Of the 66 vibrations, 33 are active in the Raman spectrum [68]. In Table 5-1, regions of different types of vibrations are given for naphthalene [70]. Because of the similarity between anthracene and naphthalene molecules, Table 5-1 can be used to identify the vibrations of anthracene.

Anthracene derivatives should have similar Raman spectra to that of anthracene. 1-Chloroanthracene (95%, Aldrich), 9-chloroanthracene (97%, Aldrich), 2-methylanthracene (97%, Aldrich), 9-methylanthracene (95%, Aldrich), 1-aminoanthracene (90%, Aldrich) were chosen for this work. All compounds used in the experiments were prepared at a concentration 10^{-4} M in acetonitrile. The anthracene

Table 5-1. Spectral regions associated with different types of vibrations.

Types of vibration	Region (cm^{-1})
CH stretching	2900-3100
CC stretching	1300-1650
CH bending in plane	1000-1500
CC bending out of plane	700-1200
CC bending in plane	<1000
CC bending out of plane	<700

derivatives, except for 1-aminoanthracene, have a strong absorption near 253.7 nm, as shown in Figure 5-1. Therefore, 1-aminoanthracene does not show a resonance Raman spectrum when excited by Hg 253.7 nm. However, the other anthracene derivatives and anthracene show Raman spectra when excited by the Hg 253.7 nm line (see Figure 5-2).

Polycyclic Aromatic Hydrocarbons

Polycyclic aromatic hydrocarbons (PAHs) are a potential hazard because some of the compounds have been shown to be carcinogens [71]. Several analytical techniques have been reviewed for the identification and quantitation of PAHs in complex matrices such as soot, water, and soil [72,73]. Resonance Raman spectrometry is used for the detection and speciation of PAHs in complex matrices. Asher's [63] group have successfully designed a UV resonance Raman spectrometer, continuously tunable between 217 and 800 nm, allowing resonance Raman excitation of the UV absorption bands of PAHs.

The incoherent resonance Raman spectrometer used in this dissertation employs a Hg Pen-Ray lamp. The Hg 253.7 nm line was the excitation wavelength. In order to obtain resonance Raman enhancement, the PAHs must have an absorption band near 253.7 nm. Triphenylene (98%, Aldrich), phenanthrene (99.5%, Aldrich), pyrene (99%, Aldrich), and fluorene (98%, Eastman) are several PAHs which were evaluated in the experiments in this dissertation. For this research, the PAHs were prepared at a concentration of 10^{-4} M, in acetonitrile. The absorption spectrum of triphenylene, with

Figure 5-1. Absorption spectra of 10^{-5} M anthracene and anthracene derivatives, in acetonitrile, measured in an 1-cm static cell.

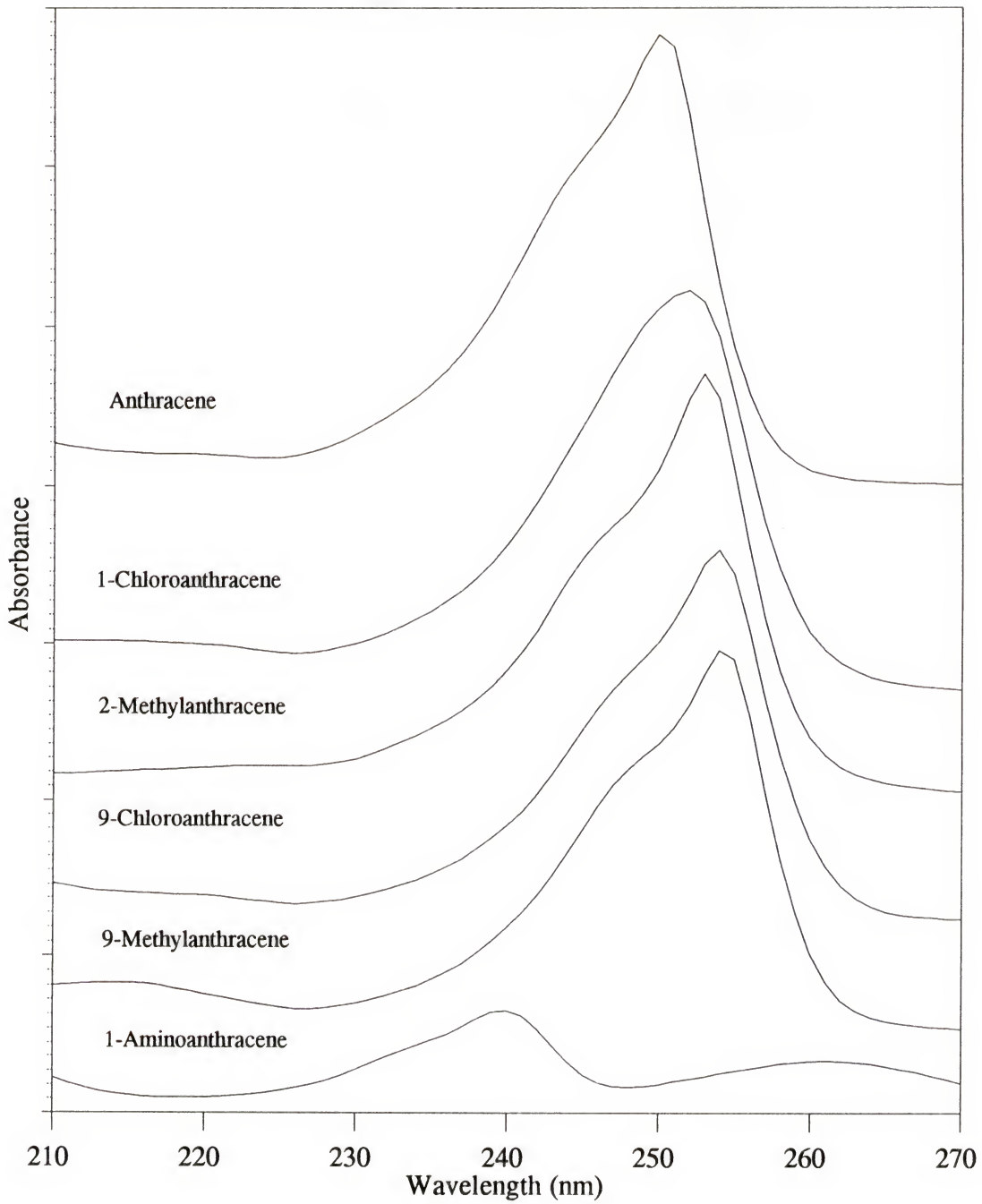
Anthracene
1-Chloroanthracene
2-Methylanthracene
9-Chloroanthracene
9-Methylanthracene
1-Aminoanthracene
Absorbance
210
220
230
240
250
260
270
Wavelength (nm)

Figure 5-2. Raman spectra of anthracene and several anthracene derivatives (all compounds at 10^{-4} M).

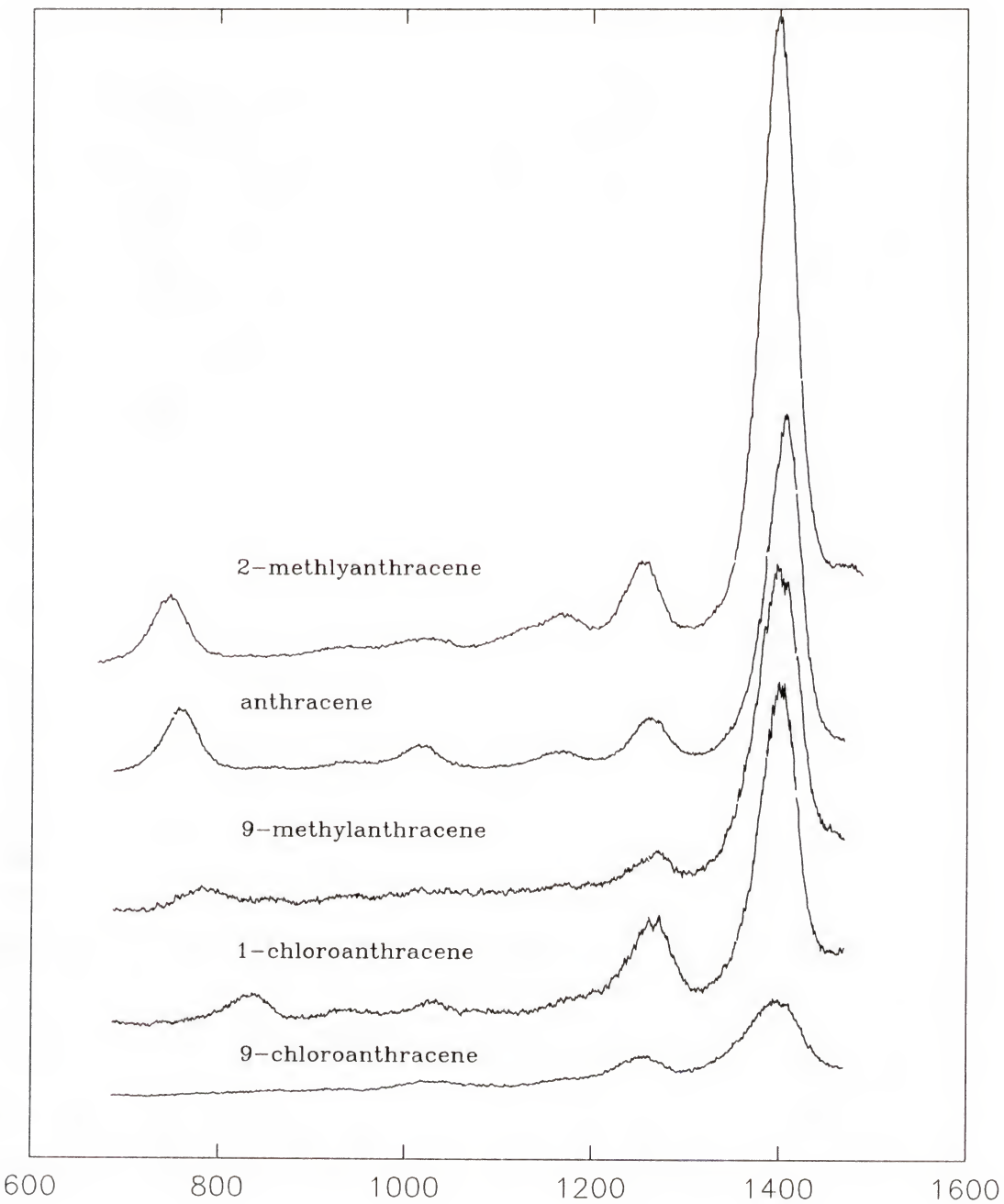
2-methlyanthracene
anthracene
9-methylanthracene
1-chloroanthracene
9-chloroanthracene
600
800
1000
1200
1400
1600

an absorption peak close to excitation source (253.7 nm) is shown in Figure 5-3. As shown in Figure 5-4, triphenylene exhibits the most intense Raman spectrum of the four compounds studied. Pyrene, with very weak absorption at the excitation wavelength, has a Raman spectrum similar to acetonitrile.

Quantitative Analysis

Quantitative resonance Raman measurements are complicated by absorption due to the incident exciting radiation and the scattered radiation. Correction methods for sample absorption have been reviewed in several papers [41,47,66,74]. Using the internal standard method, quantitative resonance Raman analysis can be simplified.

The backscattering geometry for quantitative resonance Raman spectrometry was commonly used for opaque and strongly absorbing materials. All measurements performed in this chapter involved the use of the incoherent Hg Pen-Ray lamp. This lamp is a multi-wavelength line source. It was found that backscattering and the associated noise could not be blocked by any available optical filter. Therefore, the same experimental condition described previously was used with right angle (90^0) excitation-collection. A flat piece of black cardboard was placed next to the lamp to reduce the amount of scattered light reaching the monochromator.

The Raman signal from the 756 cm^{-1} anthracene peak was selected in this resonance Raman quantitative study. The solvent peak from acetonitrile, 918 cm^{-1}, was the internal standard and was used as an indication of incident radiation intensity.

Figure 5-3. Absorption spectra of 10^{-5} M triphenylene, pyrene, phenanthrene, and fluorene, in acetonitrile, measured in an 1-cm static cuvette cell.

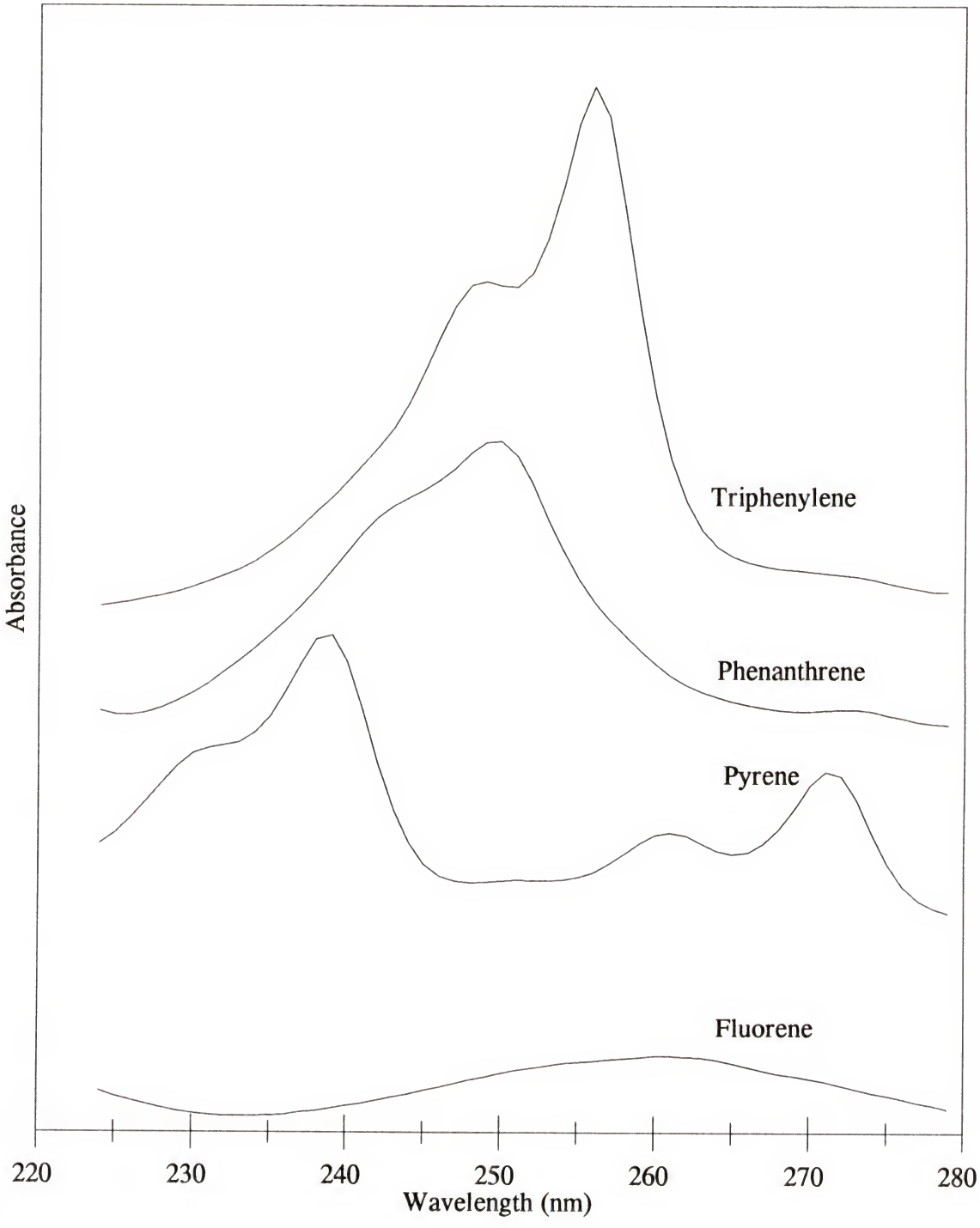
Absorbance
Triphenylene
Phenanthrene
Pyrene
Fluorene
220
230
240
250
260
270
280
Wavelength (nm)

Figure 5-4. Raman spectra of phenanthrene, triphenylene, fluorene, and pyrene (all compounds at 10^{-4} M).

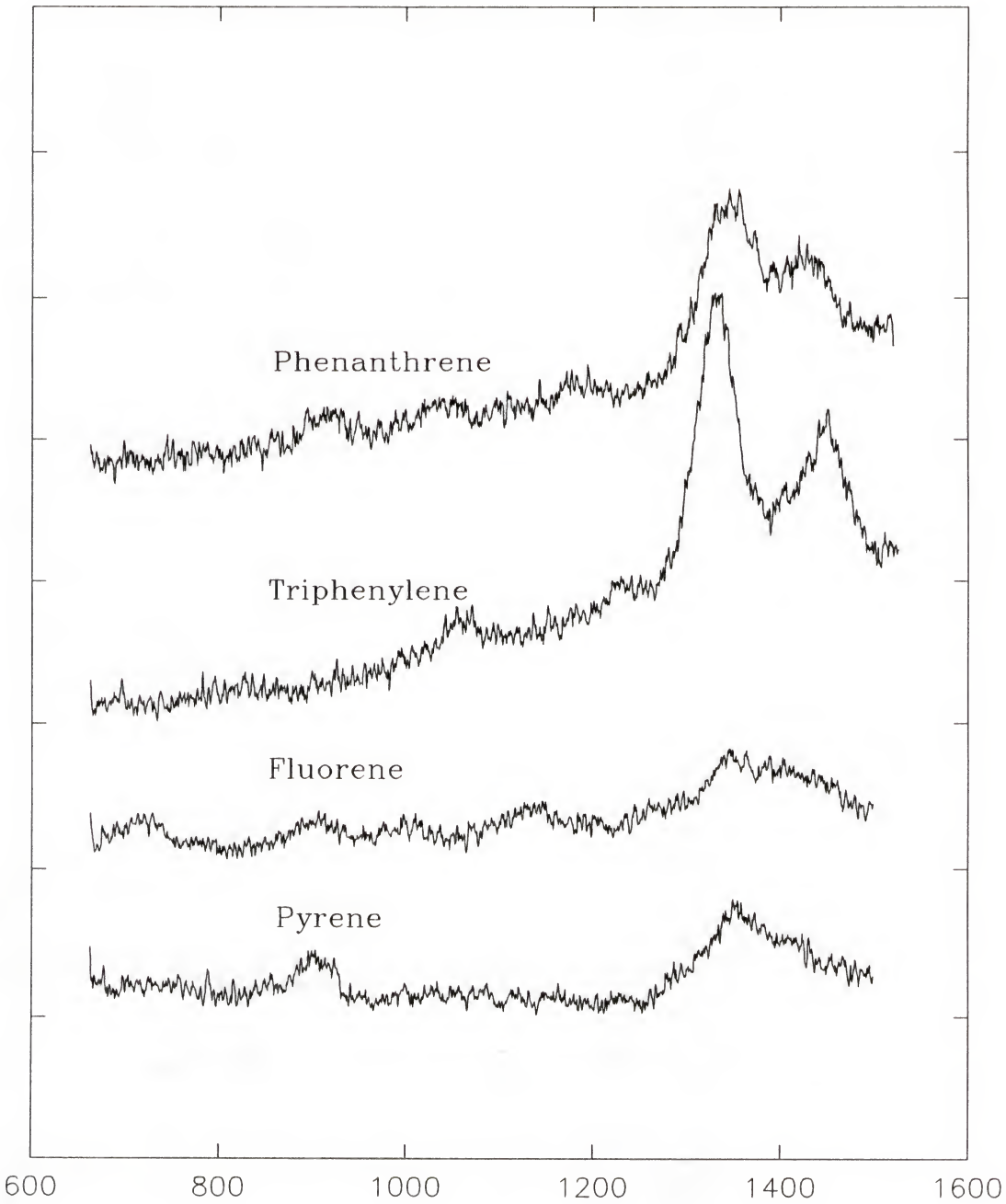
Phenanthrene
Triphenylene
Fluorene
Pyrene
600
800
1000
1200
1400
1600

Figure 5-5 shows the variation of the ratio of the anthracene Raman peak, 756 cm^{-1}, to the solvent peak, 918 cm^{-1}, versus anthracene concentration. Good linearity over about 1.2 orders of magnitude is shown. A detection limit of about 0.4 ppm was obtained.

Figure 5-5. Ratio Raman peak of anthracene, 756 cm^{-1}, corrected for source intensity, to acetonitrile Raman peak, 918 cm^{-1}, versus anthracene concentration.

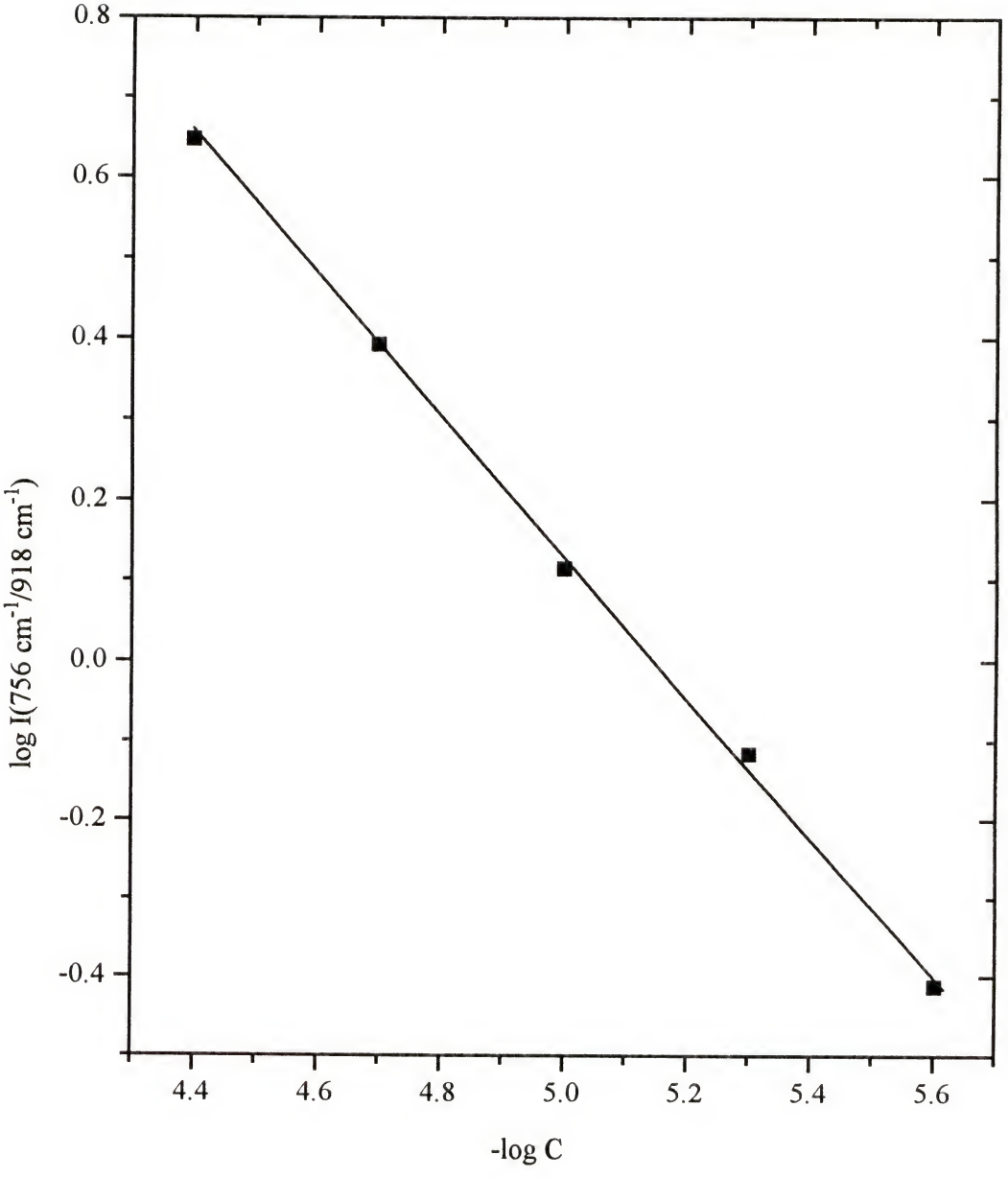
0.8
0.6
0.4
0.2
0.0
-0.2
-0.4
log I(756 cm-1/918 cm-1)
4.4
4.6
4.8
5.0
5.2
5.4
5.6
-log C

CHAPTER 6
CONCLUSIONS AND FUTURE WORK

Conclusions and Discussions

The results indicate an inexpensive and simple incoherent source has potential for application to resonance Raman spectrometry. Resonance Raman spectra of PAHs and their derivatives have been successfully measured. A detection limit of 0.4 ppm of anthracene was obtained. The Pen-Ray lamp has less selective wavelengths, low power and divergence which limits the applications to those samples which match its absorption and have a large quantity detection volume.

The Hg Pen-Ray lamp is one kind of low pressure, low current, arc source. According to previously published results, the Hg Pen-Ray lamp's current produces an optimum in the intensity of the 253.7 nm lines [75,76]. Increasing the current and pressure of the Hg Pen-Ray lamp only increases the intensity of the long wavelength line (e.g. 435.8 nm).

The sample cell is another important part of the incoherent resonance Raman spectrometer. The cell used depends on the shape of the excitation source. For example, the capillary column of index matched cell is too small for Pen-Ray lamp sources. However, this cell may be a good choice for laser sources which can easily focus onto a small area.

Future Work

Currently, the incoherent resonance Raman spectrometer is limited by the source intensity and availability of excitation wavelengths. These can be easily solved by using an intracavity Ar^+ laser. In the future, additional research into higher intensity incoherent sources which would produce different excitation lines could make this experimental setup more versatile. A metal vapor cell, which was successfully used by Pelletier [77] and Winefordner's [78] group, should be a good filter to reduce the Rayleigh light. Replacing the PMT detector with a UV-sensitive multichannel charge-coupled device (CCD) detector should improve the instrument efficiency.

REFERENCES

1 A. Smekal, *Naturwiss*, **11**, 873 (1923).

2 C.V. Raman, *Indian J. Phys.*, **2**, 387 (1928).

3 C.V. Raman and K.S. Krishnan, *Nature*, **121**, 501, 619 (1928).

4 C.V. Raman and K.S. Krishnan, *Indian J. Phsy.*, **2**, 399 (1928).

5 C.V. Raman and K.S. Krishnan, *Proc. Roy. Soc.*, **122A**, 23 (1928).

6 A. Anderson, *The Raman Effect 1*, Marcel Dekker, New York (1971).

7 G. Placzek, *Handbuch der Radiologie vol. 6*, Leipzig (1934).

8 D.H. Rank and R.V. Wiegand, *J. Opt. Soc. Am.*, **36**, 325 (1936).

9 J.G. Grasselli and E.J. Bulkin, *Analytical Raman Spectroscopy*, John Wiley & Sons, New York (1991).

10 H.L. Welsh, M.F. Crawford, T.R. Thomas and G.R. Love, *Canad. J. Phys.*, **30**, 577 (1952).

11 J.R. Ferraro, R. Jarnutowski, and D.C. Lankin, *Spectroscopy*, **7(2)**, 30 (1992).

12 T.H. Maiman, *Nature*, **187**,493 (1960).

13 S.P.S. Porto and D.L.Wood, *J. Opt. Soc. Am.*, **52**, 251 (1962).

14 R.W. Terhune, *Bull. Am. Phys. Soc.*, **8**, 359 (1963).

15 D. Landon and S.P.S. Porto, *Appl. Opt.*,**4**, 762 (1965).

16 G.W. Chantry, H.A. Gebbie, and C Hilsum, *Nature*, **203**, 1052 (1964).

17 G.F. Amelio, M.F. Tompsett, and G.E. Smith, *Bell Systems Technical Journal*, **49**, 593 (1970).

18 M. Fleischmann, P.J. Hendra, A.J McQuillan, *J. Chem. Phys. Lett.*, **26**, 163 (1974).

19 G.J. Rosasco, E.S. Etz, and W.A. Cassatt, *IVth Internat. Conf. Raman Spectros.*, Brunswick, ME, USA (1974).

20 M. Delhaye, and P. Dhamelincourt, *IVth Internat. Conf. Raman Spectros.*, Brunswick, ME, USA (1974).

21 D.E. Jennings, A. Weber, and J.W. Brault, *Appl. Opt.*, **25**, 284 (1986).

22 T. Hirschfeld and B. Chase, *Appl. Spectrosc.*, **40**, 133 (1986).

23 D.A. Long, *Raman Spectroscopy*, McGraw-Hill, New York (1977).

24 J.D. Ingle, Jr. and S.R. Crouch, *Spectrochemical Analysis,* Prentice-Hall, Englewood Cliffs, New Jersey (1988).

25 J. Behringer, *Molecular Spectroscopy, vol 3*, Chap. 3, The Chemical Society Burlington House, London (1975).

26 T.M. Niemczyk, M. Delgado-Lopez, and C.D. Newman, *Laser Focus World*, 85, March (1993).

27 H. Baranska, A. Labudzinska, and J.Terpinski, *Laser Raman SpectrometryAnalytical Applications,*John Wiley & Sons, New York (1987).

28 M.M. Carrabba, K.M. Spencer, C. Rich, and D. Rauh, *Appl. Spectrosc.*, **44**, 1558 (1990).

29 M.J. Pelletier and R.C. Reeder, *Appl. Spectrosc.*, **45**, 765 (1991).

30 Y. Taimi and R.W. Simpson, *Appl. Opt.*, **19,** 1401 (1980).

31 T.J. Mangas, A. Arribas, *Mineral MAg.*, **55**, 211 (1991).

32 B. Chase, *Anal. Chem.,* **59**, 881A (1987).

33 T. Vo-Dinh, M.Y.K. Hiromoto, G.M. Regun, and R.L. Moody, *Anal. Chem.*, **56**, 1667 (1984).

34 R.L. Garrell, *Anal. Chem.*, **61**, 401A (1989).

35 F. Ni, L. Thomas, and T.M. Cotton, *Anal. Chem.*, **61**, 888 (1989).

36 A.C. Albrecht, *J. Chem. Phys.*, **34**, 1476 (1961).

37 J. Behringer, *Molecular Spectroscopy, Vol. 2*, Chap 2, The Chemical Society, London (1974).

38 D.P. Strommen, and K. Nakamoto, *J. Chem. Educ.*, **54**, 474, (1977).

39 M.D. Morris and D.J. Wallan, *Anal. Chem.* **51**, 182A (1979).

40 H.J. Bernstein, *Phil. Trans. R. Lond.*, **A293**, 287 (1979).

41 T.J. Vickers, C.K. Mann, J. Zhu, and C.K. Chong, *Appl. Spectrosc. Rev.*, **26**, 341 (1991).

42 S.A. Asher, *Anal. Chem.*, **65**, 59A, 201A (1993).

43 D.J. Gardiner and P.R. Graves, *Practical Raman Spectroscopy,* Springer-Verlag Berlin (1989).

44. S.A. Asher, C.R. Johnson, and J. Murtaugh, *Rev. Sci. Instrum.*, **54**, 1657 (1987).

45 B. Hudson, *Spectroscopy*, **1**, 22 (1986).

46 S.A. Asher, R.W. Bormett, X.G. Chen, D.H. Lemmon, N. Cho, P. Peterson, M. Arrigoni, L.Spinelli, and J. Cannon, *Appl. Spectrosc.*, **47**, 628 (1993).

47 L.T. Lin, C.K. Mann, and T.J. Vicker, *Appl. Spectrosc.*, **41**, 422 (1987).

48 C.M. Jones, V.L. Devito, P.A. Harmon, S.A. Asher, *Appl. Spectrosc.*, **41**, 1268 (1987).

49 A.T. Tu, *Raman Spectroscopy in Biology: Principles and Applications*, John Wiley & Sons, New York (1977).

50 P.M. Champion, *Proc. SPIE-Int. Soc. Opt. Eng.*, **1055** (Raman Scattering, Lumin. Spectrosc. Instrum. Technol.), 229 (1989).

51 W.L. Peticolas, K.J. Wilson, and B.M. Britt, *Proc. SPIE-Int. Soc. Opt. Eng.*, **1057** (Biomol. Spectrosc.), 161 (1989).

52 T.G. Spiro, G. Smulevitch, and C. Su, *Biochemistry*, **29**, 4497 (1990).

53 J.L. Koenig, *Appl. Spectrosc. Rev.*, **4**, 233 (1971).

54 D.L. Gerrard and W.F. Maddams, *Appl. Spectrosc. Rev.*, **22**, 251 (1986).

55 P.M. Killough, V.L. DeVito, and S.A. Asher, *Appl. Spectrosc.*, **45**, 1067 (1991).

56 S. Chadha, E. Ghiamati, R. Manoharan, and W.H. Nelson, *Appl. Spectrosc.*, **46**, 1176 (1992).

57 K.P.J. Williams, and D.J. Klenerman, *J. Raman Spectrosc.*,**23**,191 (1992).

58 M.R. Jakupca, and P.K. Dutta, *Anal. Chem.*, **64**, 953 (1992).

59 S.A. Asher, C.R. Johnson, *Science*, **225**, 311 (1984).

60 C.R. Johnson, S.A. Asher, *Anal. Chem.*, **56**, 2258 (1984).

61 G.J. Zissis and A.J. Larocca, "Optics Radiators and Sources," in *Handbook of Optics*, W.G. Driscoll and W. Vaughan, eds., McGraw-Hill, New York, 1978.

62. G.A. Reider, K.P. Trarr, and A.J. Schmidt, *Appl. Opt.*, **23**, 2856 (1984).

63 S.A. Asher, C.R. Johnson, and J. Murraugh, *Rev. Sci. Instrum.*, **54**, 1675 (1983).

64 T.C. Strekas, D.H. Adams, A. Packer, and T.G. Spiro, *Appl. Spectrosc.*, **28**, 324 (1974).

65 M. Ludwig, and S.A. Asher, *Appl. Spectrosc.*,**42**, 1458 (1988).

66 J.D. Womack, C.K. Mann, and T.J. Vickers, *Appl. Spectrosc.*,**43**, 527 (1989).

67 D.J. Evans and D.B. Scully, *Spectrochim. Acta*, **20**, 891 (1964).

68 N. Abasbegović, N. Vukotić, and L. Colombo, *J. Chem. Physic.*, **41**, 2575 (1964).

69 N. Neto, M. Scrocco, and S. Califano, *Spectrochim. Acta*, **22**, 1981 (1966).

70 E. Lippincott and E. O'Reilly, *J. Chem. Phys.*, **23**, 238 (1955).

71 C. Heidelberger, *Annu. Rev. Biochem.*,**44**, 79 (1975).

72 A. Bjørseth, Ed., *"Handbook of Polycyclic Aromatic Hydrocarbons,"* Marcel Dekker, New York (1983).

73 T. Vo-Dinh, Ed., *"Chemical Analysis of Polycyclic Aromatic Compounds,"* John Wiley & Sons, New York (1988).

74 S.A. Asher, *Anal. Chem.*, **56**, 720 (1984).

75 C.B. Childs, *Appl. Opt.*, **1**, 711 (1962).

76 Pen-Ray Lamps catalogue from Ultra-Violet Products, Inc., San Gabriel, California, No. **109B**.

77 M.J. Pelletier, *Appl. Spectrosc.*, **46**, 395 (1992).

78 R. Indralingam, J.B. Simeonsson, G.A. Petrucci, B.W. Smith, and J.D. Winefordner, *Anal. Chem.*, **64**, 964 (1992).

BIOGRAPHICAL SKETCH

Chonyu Chen was born on August 15, 1960, in Yun-Lin county, Taiwan. He obtained his B.Sc. degree in chemistry from the National Cheng Kong University, Tainan, Taiwan, and is currently a graduate student in the Department of Chemistry, University of Florida.

I certify that I have read this study and that in my opinion it conforms to acceptable standards of scholarly presentation and is fully adequate, in scope and quality, as a dissertation for the degree of Doctor of Philosophy.

James D. Winefordner, Chairman
Graduate Research Professor of
Chemistry

I certify that I have read this study and that in my opinion it conforms to acceptable standards of scholarly presentation and is fully adequate, in scope and quality, as a dissertation for the degree of Doctor of Philosophy.

Anna Brajter-Toth
Associate Professor of Chemistry

I certify that I have read this study and that in my opinion it conforms to acceptable standards of scholarly presentation and is fully adequate, in scope and quality, as a dissertation for the degree of Doctor of Philosophy.

John Eyler
Professor of Chemistry

I certify that I have read this study and that in my opinion it conforms to acceptable standards of scholarly presentation and is fully adequate, in scope and quality, as a dissertation for the degree of Doctor of Philosophy.

Joseph Delfino
Professor of Environmental
Engineering Sciences

This dissertation was submitted to the Graduate Faculty of the Department of Chemistry in the College of Liberal Arts and Sciences and to the Graduate School and was accepted as partial fulfillment of the requirements for the degree of Doctor of Philosophy.

April, 1994

_____

Dean, Graduate School